Modelling of 3D microstructure and effective diffusivity of fly ash blended cement paste

Cheng Liu [a], Fazhou Wang [b], Mingzhong Zhang [a,*]

[a] Department of Civil, Environmental and Geomatic Engineering, University College London, London, WC1E 6BT, UK

[b] State Key Laboratory of Silicate Materials for Architecture, Wuhan University of Technology, Wuhan, 430070, China

Abstract: Accurate prediction of microstructural evolution and ionic diffusivity in fly ash blended cement paste is significant for practical application and durability design of blended cementitious materials. This paper presents an integrated modelling framework for simulating 3D microstructure and effective ionic diffusivity of blended cement paste with various fly ash replacement levels and w/b ratios. A voxel-based hydration model using cellular automaton-like evolution rules was developed to simulate 3D microstructural development of fly ash blended cement, based on which the effective diffusivity was simulated using a lattice Boltzmann (LB) model for diffusion considering the contributions of both capillary pores and gel pores in C-S-H gels to ionic diffusion. A series of experiments were conducted to characterise the morphology of Portland cement and fly ash, hydration process and pore structure of fly ash blended cement paste and measure the effective ionic diffusivity. The simulation results agree well with experimental data in terms of hydration heat, calcium hydroxide content, degree of hydration of fly ash, porosity, and effective diffusivity, which suggests that the developed microstructure-based LB model for diffusion can predict the ionic diffusivity of fly ash blended cement paste with high accuracy. The addition of fly ash can help reduce the ionic diffusivity of cement paste particularly after the capillary porosity depercolation occurs due to the more tortuous diffusion paths in the pozzolanic C-S-H gels.

Keywords: Fly ash; Hydration model; Lattice Boltzmann method; Pore structure; Percolation; Diffusivity

1. Introduction

Fly ash is an industrial byproduct from the coal combustion at thermal power plants. If properly used, partial replacement of Portland cement clinkers with fly ash can not only promote the sustainability of cementitious materials via significant reduction of CO_2 emissions, but also improve the properties of cementitious materials, e.g., rheological, mechanical and transport properties [1-3]. Fly ash is much less reactive than Portland cement clinker but would accelerate the rate of hydration of cement clinker in blended cement due to the dilution effect [4], heterogeneous nucleation effect [5] and surface absorption effect [6]. Fly ash particles with spherical geometry acting as "ball-bearing" can enhance the rheological properties of fresh paste [7]. More importantly, because of the presence of amorphous

* Corresponding author. E-mail address: mingzhong.zhang@ucl.ac.uk (M. Zhang)

silicate and aluminate phases, fly ash possesses potential pozzolanic effect [7-9]: during the hydration process of cement, the glass phases react with calcium hydroxide (CH) to form calcium silicate hydrate (C-S-H) and calcium aluminate hydrate (C-A-H). Accordingly, the microstructure of hardened cement paste is modified with the continuous formation of pozzolanic hydration products, transition of C-S-H gel, and refinement of pore structure.

To acquire the 3D microstructure of fly ash blended cement paste, some advanced characterization techniques including X-ray computed tomography (XCT) [10] and laser scanning confocal microscopy (LSCM) [11] were used. Lu et al. [10] applied XCT to obtain the microstructure of fly ash blended cement paste with a resolution of 4 μm/voxel and found that the porosity and connectivity of pore structure of fly ash blended cement paste are lower than those of plain cement paste. Nevertheless, the microstructural information obtained from XCT is highly restricted by the spatial resolution. The phases with a size smaller than the used resolution (e.g. small capillary pores and gel pores) cannot be accurately detected. Yio et al. [11] acquired the 3D pore structure of fly ash blended cement paste using LSCM with a resolution of 0.105 μm/voxel and observed that the incorporation of fly ash can help reduce the volume, size and connectivity of accessible pore network and increase the pore tortuosity and formation factor of hardened cement paste. However, apart from the microstructural change induced by the sample preparation, the imaging depth of LSCM is very small, which limits its ability to accurately acquire a representative microstructure of fly ash blended cement paste [12]. Moreover, XCT and LSCM tests are usually time-consuming and expensive. It is still a great challenge to accurately capture the 3D microstructure of fly ash blended cement paste through experiments. To tackle these drawbacks, several computer-based models have been developed to simulate the hydration process and microstructural development of fly ash blended cement paste on the basis of hydration models for pure Portland cement system, such as CEMHYD3D [13], HYMOSTRUC3D [14], μic [15] and DuCOM [16]. For instance, Bentz [17] incorporated fly ash into the pixel-based CEMHYD3D model to simulate the hydration and microstructure evolution of fly ash blended cement paste using a cellular automaton-like evolution rule. However, this model has not yet been validated by experiments and some parameters in the model were not well considered and in need of further improvement [18]. Following the similar kinetic equations suitable for Portland cement, Gao [19] extended the HYMOSTRUC3D model for fly ash blended cement considering the features of pore solution and the distribution of CH phase in the microstructure. Nevertheless, the extended model neglects the interaction between fly ash and CH. Bishnoi et al. [20] used the μic model to simulate the microstructure of fly ash blended cement paste and investigated the effect of fly ash on its strength without any verifications of hydration process with experimental data. Wang et al. [21] modified the DuCOM model to simulate the hydration process of fly ash blended cement considering the contribution of cement hydration and reactions of fly ash to the heat release rate. The

simulation results showed good agreement with experimental data. However, the proposed model was only focused on the simulation of hydration process and the microstructure development has not been presented. Therefore, it is necessary and vital to investigate the 3D microstructure of fly ash blended cement pate using a suitable hydration model.

The diffusivity of fly ash blended cement paste is highly associated with its microstructure and is a critical parameter for the assessment of durability and prediction of service life of concrete infrastructure made of fly ash blended cementitious materials [22]. The diffusivity of cementitious materials can be measured using natural diffusion tests or electrically accelerated methods [23]. However, it was found that there is significant difference in the measured diffusivity values through different methods and there is still no agreement on the standardized measurement of diffusivity [24]. In addition, due to the dense pore structure and less penetration, it is very difficult to accurately measure the diffusivity of fly ash blended cement paste, particularly at later ages. In the past few years, some empirical equations as well as analytical and numerical models have been proposed to predict the diffusivity of fly ash blended cement paste. Through fitting of experimental data, empirical equations were generally established to describe the relationship between diffusivity and porosity of fly ash blended cement paste. For example, Ampadu et al. [25] reported that there is a linear correlation between diffusivity on a log scale and porosity and the correlation is better for fly ash blended cement paste compared to Portland cement paste. Nokken and Hooton [26] demonstrated that the quantitative relationship between diffusivity and porosity conforms to the Archie's law (exponential function) but the constants of the Archie's law for Portland and fly ash blended cement pastes vary over a wide range. Despite the simplicity and ease application, the detailed microstructure characteristics including morphology, connectivity and tortuosity of the pore structure were not taken into consideration in the established empirical models. Moreover, the fitting parameters in the empirical equations merely denote optimal values for best fits and have no physical meaning.

In terms of analytical models, the relationship was established considering the morphology of pore structure in fly ash blended cement paste that was conceptualized into the geometrical configurations. Many analytical methods have been successfully employed to predict diffusivity of fly ash blended cement paste. Oh and Jang [27] proposed a general effective medium model to estimate the effective diffusivity in fly ash blended cement paste, which can well predict the diffusivity near the percolation threshold of capillary porosity. Similarly, Zhou et al. [28] presented an effective medium model to evaluate the effective diffusivity in fly ash blended cement paste based on the characteristic parameters of pore structure. The diffusivity in fly ash blended cement paste with various curing ages, water-to-binder (w/b) ratios and fly ash replacement ratios was predicted using this model, which agrees well with experimental results. Different from the empirical models, some influencing parameters can be considered in the analytical models. Nevertheless, the analytical

models may fail in some situations, e.g., the dramatically varying diffusivity of different phases and the very high content of diffusive phases in microstructure [29-31]. In contrast to empirical equations and analytical models, numerical models for predicting effective diffusivity show a great potential in terms of taking the complex microstructure of cement paste into consideration. Among the existing numerical models, the model for predicting diffusivity based on the virtual cement paste is more popular because the influences of different factors can be easily incorporated into the model. Based on the Nernst-Einstein equation, Garboczi and Bentz [32] simulated the diffusivity of virtual hydrating Portland cement paste with various water-to-cement (w/c) ratios generated by CEMHYD3D using finite difference and finite element methods. Zhang et al. [33,34], Liu et al. [35], and Ukrainczyk and Koenders [36] respectively developed the in-house lattice Boltzmann, random walk, and finite difference codes to simulate the ionic diffusivity of Portland cement paste at various curing ages, w/c ratios, and water saturation levels obtained using HYMOSTRUC3D. The simulated results of diffusivity showed good agreement with experimental data. However, to the best of the authors' knowledge, the existing numerical models were only applied to Portland cement paste and the numerical simulations of effective diffusivity in fly ash blended cement paste have been rarely conducted. Therefore, it is vital to propose a suitable numerical model to fill this gap.

To this end, the main purpose of this study is to simulate the hydration process and microstructural development of fly ash blended cement paste as well as the ionic diffusivity based on the generated virtual 3D microstructure. Firstly, a modified version of the hydration model CEMHYD3D along with cellular automaton-like evolution rules was developed to simulate the evolution of 3D microstructure of fly ash blended cement paste, which was validated with experimental data in terms of hydration heat, CH content, degree of hydration of fly ash, and porosity. Afterwards, the diffusion of ions through the generated fly ash blended cement paste was simulated using lattice Boltzmann (LB) method. The effective ionic diffusivity was then predicted and compared with experimental data. Finally, the effects of different factors including fly ash content, curing ages and w/b ratios were estimated in a quantitative manner.

2. Modelling of 3D microstructure of fly ash blended cement paste

2.1. Theory of hydration of fly ash blended cement system

Portland cement is composed of four mineral phases, i.e., C_3S, C_2S, C_3A and C_4AF. When cement is mixed with water, C_3S and C_2S react with water to form hydration products, i.e. C-S-H and CH, while C_3A and C_4AF contribute to the generation of C_3AH_6 and FH_3. To control the setting rate of cement paste, the cement clinker is normally grounded with 4-6% gypsum ($C\bar{S}H_2$). In this situation, the hydration products related to C_3A and C_4AF become more complicated, because the reactions of C_3A and C_4AF depend on the content of gypsum. C_3A and C_4AF can react with $C\bar{S}H_2$ and water to form ettringite ($C_6A\bar{S}_3H_{32}$). If $C\bar{S}H_2$ is consumed up, C_3A and C_4AF will further react with $C_6A\bar{S}_3H_{32}$ and

water to form AFm ($C_4A\bar{S}H_{12}$). The classical chemical reactions (i.e. hydration) of Portland cement can be summarized as follows [37,38]:

$$C_3S + 5.3H \rightarrow C_{1.7}SH_{3.9} + 1.3CH \quad (1)$$

$$C_2S + 4.3H \rightarrow C_{1.7}SH_{3.9} + 0.3CH \quad (2)$$

If there is no $C\bar{S}H_2$,

$$C_3A + 6H \rightarrow C_3AH_6 \quad (3)$$

$$C_4AF + 10H \rightarrow C_3AH_6 + CH + FH_3 \quad (4)$$

If $C\bar{S}H_2$ is present,

$$C_3A + 3C\bar{S}H_2 + 26H \rightarrow C_6A\bar{S}_3H_{32} \quad (5)$$

$$2C_3A + C_6A\bar{S}_3H_{32} + 4H \rightarrow 3C_4A\bar{S}H_{12} \quad (6)$$

$$C_4AF + 2C\bar{S}H_2 + 30H \rightarrow C_6A\bar{S}_3H_{32} + CH + FH_3 \quad (7)$$

$$2C_4AF + C_6A\bar{S}_3H_{32} + 12H \rightarrow 3C_4A\bar{S}H_{12} + 2CH + 2FH_3 \quad (8)$$

In the presence of fly ash, the amorphous silicate and aluminate phases in fly ash can react with the hydration product, i.e. CH, to form C-S-H with a low Ca/Si ratio and C-A-H. Although the pozzolanic effect has been widely confirmed, the hydration products and their specific compositions are not unified [17,39,40]. For example, Helmuth [39] proposed the following chemical reactions of fly ash in Portland cement system:

$$aCH + bS + cH \rightarrow C_aS_bH_c \quad (9)$$

$$AS_2 + CH + cH \rightarrow CSH_{c-5} + C_2ASH_8 \quad (10)$$

$$A + 3CH + C\bar{S}H_2 + 7H \rightarrow C_4A\bar{S}H_{12} \quad (11)$$

Afterwards, Bentz et al. [17] investigated the chemical composition of fly ash and recommended the following chemical reaction equations for fly ash blended cement system:

$$S + 1.1CH + 2.8H \rightarrow C_{1.1}SH_{3.9} \quad (12)$$

$$AS + 2CH + 6H \rightarrow C_2ASH_8 \quad (13)$$

$$CAS_2 + C_3A + 16H \rightarrow 2C_2ASH_8 \quad (14)$$

$$CAS_2 + C_4AF + 20H \rightarrow 2C_2ASH_8 + CH + FH_3 \quad (15)$$

$$C\bar{S} + 2H \rightarrow C\bar{S}H_2 \quad (16)$$

According to research presented by Papadakis [40], the reaction products resulted from pozzolanic reaction of fly ash are composed of C-S-H, C_4AH_{13} and $C_4A\bar{S}H_{12}$, the detailed chemical reactions of which can be expressed as:

$$S + 1.5CH + 1.5H \rightarrow C_{1.5}SH_{1.5} \quad (17)$$

$$A + 3CH + C\bar{S}H_2 + 7H \rightarrow C_4A\bar{S}H_{12} \quad (18)$$

$$A + 4CH + 9H \rightarrow C_4AH_{13} \quad (19)$$

The Ca/Si ratio of C-S-H was found to be different in different studies. In addition, Helmuth [39]

and Bentz et al. [17] assumed that strätlingite (C_2ASH_8) can be produced, while Papadakis [40] thought that aluminate hydrate (C_4AH_{13}) can be produced. The different pozzolanic reaction products can be attributed to the difference in chemical composition of fly ash investigated in their studies. In this study, the chemical reactions proposed by Bentz et al. [17] were used to develop a hydration model for fly ash blended cement system, because the hydration products given in [17] have specific composition and fly ash particles consisting of multiple phases that are close to the real situation [41].

2.2. Modelling of hydration of fly ash blended cement

In the past few decades, numerous hydration models for Portland cement system have been proposed and widely used. To build a hydration model for fly ash blended cement system, the optimal way would be the extension of these existing models suitable for Portland cement as they have been well validated. In this study, the CEMHYD3D hydration model based on cellular automaton-like evolution rules with open-source code was selected and modified by considering the influence of fly ash on cement hydration according to the theory introduced in Section 2.1. The details about the simulation of hydration and microstructure development of Portland cement using CEMHYD3D can be found in [13].

The entire module for simulating hydration process and microstructure evolution of fly ash blended cement paste consists of three main parts, i.e., cement packing, phase segmentation, and hydration, as illustrated in Fig. 1. Regarding cement packing, the digital representative volume element (RVE) with size of 200×200×200 μm^3 (rather than 100×100×100 μm^3 that was widely applied for Portland cement systems [20,42-44]) and a resolution of 1 μm/voxel is used to avoid the potential size effect. Based on the inputs, e.g., particle size distribution, w/b ratio and fly ash replacement ratio, the packing of cement and fly ash particles was achieved using Monte Carlo simulation. Here, the particles cannot overlap with each other and the packing sequence is from the largest particles to the smallest ones. It should be mentioned that the shape of Portland cement can be set as irregular shape [45,46]. However, to control the number of variables in this study, the shapes of cement and fly ash were regarded as sphere for simplification, as it has been found that the initial shape of cement powders has negligible effects on the microstructural characteristics [45-47] and properties of hardened cement paste, e.g. diffusivity [48].

After obtaining the 3D packed structure, the cement and fly ash particles were segmented into various mineral phases. Cement particles were divided into pixels of C_3S, C_2S, C_3A and C_4AF using a sintering algorithm according to the bulk phase composition and auto-correlation functions of the mineral phases [13], while fly ash particles are composed of multi-phases, i.e., amorphous phases (S, A-S and C-A-S) and crystalline phases (mullite, quartz and other non-reactive phases). Following Bentz's assumption [17], fly ash particles were regarded as a combination of S, AS, CAS_2 and inert phase. This assumption has been confirmed by Chancey et al. [49] and Durdziński et al. [50], who

found that fly ash consists of basic glass phases, i.e., glass silicate, aluminate-silicate and calcium-aluminate-silicate. To place each phase on the fly ash particles, two different ways were proposed based on the characteristics of fly ash: One is to use the sintering algorithm, similar to the segmentation of cement clinkers; The other one is to divide fly ash particles into individual phases according to the volume fraction of each phase. A typical example of the segmented fly ash particles using the second segmentation method is shown in Fig. 1.

After the pre-hydrated cement paste was reconstructed, the cellular automaton-like evolution rules were applied to simulate the hydration process using CEMHYD3D considering the pre-defined dissolution and reaction probabilities as well as the volume stoichiometry and physical and chemical characteristics of Portland cement and fly ash, according to Eqs. (1)-(8) and Eqs. (12)-(16), respectively. It is defined in CEMHYD3D that the cement phase voxels can dissolve, diffuse within capillary pores, and react to produce solid hydration products through a series of dissolution, diffusion and reaction cycles according to Eqs. (1)-(8). To correlate the real time (t) with computational cycles (n), a Knudsen diffusion-based equation given below was used:

$$t = \beta n^2 \tag{20}$$

where β is a conversion factor that is normally set to 0.00035 [13,18,51].

The reactions of Portland cement can be well simulated using cellular automaton-like evolution rules incorporated into the original CEMHYD3D model, which are directly followed for simulating cement hydration in this study. With respect to fly ash, three new diffusing species were introduced, i.e., diffusing S, diffusing AS and diffusing CAS_2. Similar to the cellular automaton-like evolution rules for Portland cement [13], the interactions between these new diffusing species and the phases of Portland cement are defined as follows: (1) when the diffusing S species collide with either solid or diffusing CH, $C_{1.1}SH_{3.9}$ is formed; (2) when the diffusing AS species collide with either solid or diffusing CH, C_2ASH_8 is formed; (3) when the diffusing CAS_2 species collide with either solid or diffusing C_3A, C_2ASH_8 is formed; if they collide with solid C_4AF, C_2ASH_8, CH and FH_3 are formed. To capture the released heat, the normalised released heat of reacted fly ash was used to calculate the released heat of fly ash blended cement paste, which is found to be 210 J/g for fly ash [21,52].

The pozzolanic reaction of fly ash is highly dependent on pH and temperature. To reflect the effects of pH and temperature on the reaction rate of fly ash, the empirical equations applied to cement clinkers in original CEMHYD3D [13] were extended for fly ash reaction. The following equation was introduced to adjust the dissolution probability of fly ash.

$$P_{iFA} = P_{iFA}^0 \frac{1}{1+f_{pH}} \tag{21}$$

where P_{iFA} is the dissolution probability of glass phase i in fly ash, P_{iFA}^0 is the basic dissolution probability at the initial state that is a pre-defined value, and f_{pH} is a factor related to pH as follows:

$$f_{pH} = \begin{cases} 1.0 & pH < 12.75 \\ 0.667 & pH \geq 12.75 \\ 0.333 & pH \geq 13.00 \\ 0 & pH \geq 13.25 \\ -0.25 & pH \geq 13.75 \end{cases} \quad (22)$$

The effect of temperature on the reaction rate of fly ash was introduced using the following equations:

$$P_{iFA} = P_{iFA}^{0} \frac{k_{FA}}{k_C} \quad (23)$$

$$k_C = exp\left[-\frac{1000E_C}{R}\left(\frac{1}{T+273.15} - \frac{1}{298.15}\right)\right] \quad (24)$$

$$k_{FA} = exp\left[-\frac{1000E_{FA}}{R}\left(\frac{1}{T+273.15} - \frac{1}{298.15}\right)\right] \quad (25)$$

where k_C and k_{FA} are the factors of Portland cement and fly ash associated with temperature, E_C and E_{FA} are the activation energies for Portland cement (40 kJ/mol) and fly ash (80 kJ/mol) [13], and T is temperature.

The pre-defined basic dissolution probabilities for S, AS and CAS_2 were all set as 0.08 that was determined by fitting the experimental data (see Section 5.1) and found to be far smaller than that for cement clinkers, e.g., 0.7 for C_3S.

3. Modelling of effective diffusivity of fly ash blended cement paste

3.1. Lattice Boltzmann simulation of effective diffusivity

LB method originates from the kinetic Boltzmann equation, which treats the fluid as an assemble of artificial particles and explores the microscopic features of the fluid considering collisions between particles. It has already achieved considerable success in simulating fluid flow and ionic transport in porous media because of its easy implementation of multiple interparticle interactions and complex geometry and boundary conditions. In this study, a LB model for diffusion was proposed to simulate the effective diffusivity in fly ash blended cement paste, the basic theory of which is briefly introduced here. In addition, the benchmark tests were carried out to validate the LB diffusion model.

For the pure diffusion in porous media without advection or chemical reaction, the discretized Boltzmann equation can be expressed as:

$$f_\alpha(\mathbf{x} + \mathbf{e}_\alpha \delta t, t + \delta t) - f_\alpha(\mathbf{x}, t) = -\frac{1}{\tau_i}\left[f_\alpha(\mathbf{x}, t) - f_\alpha^{eq}(\mathbf{x}, t)\right] \quad (26)$$

where f_α is the particle distribution function at lattice location $\mathbf{x}$ and time t, δt is the time step, τ_i is the non-dimensional relaxation time for diffusive phase i, $\mathbf{e}_\alpha$ is the discrete lattice velocity, the subscript $\alpha = 0, 1, \ldots (b\text{-}1)$ denotes the velocity direction where b is the number of the discrete lattice velocity directions, and f_α^{eq} is the equilibrium particle distribution function that is expressed as:

$$f_\alpha^{eq}(\mathbf{x}, t) = \frac{1}{b} c(\mathbf{x}, t) \quad (27)$$

where $c(\mathbf{x}, t)$ is the ionic concentration, accounting for the number of particles, i.e. $c(\mathbf{x}, t) =$

$\sum_\alpha f_\alpha(\mathbf{x}, t)$.

In general, the LB simulation of transport phenomena in 3D porous media requires a cubic lattice model with 19 discrete velocity directions, i.e. D3Q19. However, it has been demonstrated that when the discrete velocity directions decrease from 19 to 7, i.e. from D3Q19 to D3Q7, it can still provide high accuracy for the simulation of the pure diffusion without advection or chemical reaction [53]. The reduction of the discrete velocity directions can significantly increase the computational efficiency and reduce the required computational cost. Thus, the D3Q7 cubic lattice model shown in Fig. 2 is used in this study. The corresponding lattice velocity vector of the D3Q7 model is:

$$\mathbf{e}_\alpha = \begin{bmatrix} 0 & v & -v & 0 & 0 & 0 & 0 \\ 0 & 0 & 0 & v & -v & 0 & 0 \\ 0 & 0 & 0 & 0 & 0 & v & -v \end{bmatrix} \tag{28}$$

where v is the diffusion lattice speed, equal to $\delta x/\delta t$, and δx represents the lattice spacing.

v can be set to any positive value as long as $\tau_i \in (0.5, 2)$ [54]. For the D3Q7 model, the non-dimensional relaxation time τ_i for pure diffusion is associated with the diffusivity of the corresponding phase ($\widetilde{D}_i$) in lattice units as:

$$\widetilde{D}_i = \frac{2}{7}\left(\tau_i - \frac{1}{2}\right)\frac{(\delta x)^2}{\delta t} \tag{29}$$

Regarding the LB simulation of pure diffusion, the entire process involved in Eq. (26) contains two steps, including collision step and streaming step, which can be described by Eq. (30) and Eq. (31), respectively.

$$\bar{f}_\alpha(\mathbf{x}, t) - f_\alpha(\mathbf{x}, t) = -\frac{1}{\tau_i}\left[f_\alpha(\mathbf{x}, t) - f_\alpha^{eq}(\mathbf{x}, t)\right] \tag{30}$$

$$f_\alpha(\mathbf{x} + \mathbf{e}_\alpha \delta t, t + \delta t) = \bar{f}_\alpha(\mathbf{x}, t) \tag{31}$$

where f_α and $\bar{f}_\alpha$ represent the pre- and post-collision states of the particle distribution function.

After reaching the steady state (based on the given criterion in Eq. (34)), the diffusive flux across the porous medium ($\tilde{J}$) can be calculated from the particle distribution function:

$$\tilde{J} = \sum_\alpha \mathbf{e}_\alpha f_\alpha \frac{\tau_i - 0.5}{\tau_i} \tag{32}$$

The diffusivity of porous medium ($\widetilde{D}_e$) in lattice units can be subsequently calculated according to the following statistical equation proposed by Xuan et al. [55]:

$$\widetilde{D}_e = \widetilde{D}_0 \frac{\tilde{J}}{\tilde{J}_0} \tag{33}$$

where $\widetilde{D}_0$ is the ionic diffusivity in bulk water in lattice units, $\widetilde{\tilde{J}_0}$ is diffusive flux across a water-saturated pore space with the same size as the porous medium.

In this study, the dimensional lattice length and time were set as $\delta x = 1$ and $\delta t = 1$, and the relaxation time of water-saturated pore was regarded as 1, i.e. $\tau_0 = 1$. According to Eq. (29), $\widetilde{D}_0 = \frac{1}{7}$. It should be mentioned that the lattice units were used in LB method and it is necessary to establish

a mapping between the lattice units and real physical units. The lattice coordinates $(\mathbf{x}, t)$ are related to the physical coordinates $(\mathbf{X}, T)$ by $\mathbf{X} = L_0\mathbf{x}$ and $T = T_0 t$, where L_0 and T_0 are length and time mapping, respectively. For example, since the digital resolution of simulated cement paste is 1 μm/voxel, i.e. $L_0\delta x = 1\ \mu m = 10^{-6}$ m, L_0 is equal to 10^{-6} m. The ionic diffusivity in bulk water (D_0) is 2.03×10^{-9} m^2/s [56] with dimensions $[L]^2[T]^{-1}$, so the relationship between $\widetilde{D}_0$ and D_0 is $D_0 = \widetilde{D}_0 L_0^2 T_0^{-1}$. Thus, we can get T_0 = 7.037×10^{-5} s, and the conversion between the simulated results in lattice units and the corresponding quantities in real physical units can be established.

Cement paste is a complex heterogeneous material, consisting of two diffusive phases, i.e., capillary pore and C-S-H containing gel pore, and multiple non-diffusive phases, i.e., unreacted binders, gypsum, and crystalline hydration products [32-36]. To validate the feasibility of LB diffusion model for cement paste, the benchmark tests on ionic diffusion in a dual-component medium with two basic structures, including parallel structure and series structure were carried out. Fig. 3 shows a schematic diagram of the ionic diffusion in X-direction of parallel structure and series structure. The size of 3D dual-component medium is 100×100×100 lattices, and the diffusivities of components 1 and 2 were set as D_1 and D_2 (D_1>D_2 and D_1 = 1 m^2/s). The theoretical solutions of the ionic diffusivity in such dual-component medium can be expressed as $(D_1 + D_2)/2$ for parallel structure and $1/(1/2D_1 + 1/2D_2)$ for series structure [54].

For LB simulation, the relaxation time of component 1 (τ_1) and component 2 (τ_2) as inputs should be determined in advance that are related to the relative diffusivity, i.e. $D_2/D_1 = \left(\tau_2 - \frac{1}{2}\right)/\left(\tau_1 - \frac{1}{2}\right)$. For example, supposing $\tau_1 = 1$, τ_2 is calculated to be 0.505 for D_2/D_1 = 0.01. In terms of the boundary condition, the periodic boundary condition was adopted in the diffusion direction, i.e. X-direction (see Fig. 3). The ionic concentrations on the inlet and outlet surfaces were set as 1.0 mol/L and 0 mol/L, respectively. Regarding the other four surfaces, it was assumed that there is no diffusive flux through them, and the half-way bounce-back condition was applied to the interface between diffusive and non-diffusive phases. The steady-state diffusion criterion is defined based on the ionic concentration at the position i at two consecutive time steps (i.e. c_i^{n+1} and c_i^n) as follows:

$$\frac{\sum_i |c_i^{n+1} - c_i^n|}{\sum_i |c_i^{n+1}|} < 10^{-8} \tag{34}$$

This criterion is found to not only guarantee the accuracy of computational accuracy but also save the computational time and memory requirements. After reaching the steady state, the overall diffusive flux through the medium as well as the ionic diffusivity can be calculated using Eqs. (32) and (33). A typical example of the steady-state distribution of ionic concentration in the dual-component medium with D_2/D_1=0.01 is shown Fig. 4. The comparison between simulated results and theoretical results for various D_2/D_1 ratios ranging from 0.0001 to 0.5 is presented in Table 1. The maximum discrepancy between simulation and theoretical results is less than 0.015% for the

parallel mode and 0.5% for the series mode, respectively, suggesting that the proposed LB diffusion model can provide a good prediction for the effective diffusivity in the heterogeneous medium.

3.2. Determination of input parameters

As mentioned above, there are two diffusive phases in the heterogeneous cement paste, i.e., capillary pore and porous C-S-H gels containing gel pores [32-36]. It is necessary to quantify their diffusivities as inputs for LB simulation of ionic diffusivity in cement paste. The ionic diffusivity of capillary pore (D_0) is equal to 2.03×10^{-9} m^2/s [56]. Porous C-S-H is composed of basic colloidal particles and gel pores [57], and its ionic diffusivity is highly dependent on the gel porosity of C-S-H. According to the colloidal structure of C-S-H [57], the relationship between the tortuosity of C-S-H (μ_D) and the gel porosity of C-S-H (ϕ_{CSH}) can be described by [58]:

$$\frac{1}{\mu_D} = 0.059 + 0.226(\phi_{CSH})^{2.68} \quad (35)$$

And, the diffusivity of C-S-H (D_{CSH}) relative to that of pore solution in gel pore of C-S-H (D_{GP}) can be expressed as [46]:

$$\frac{D_{CSH}}{D_{GP}} = \frac{1}{\mu_D}\phi_{CSH} \quad (36)$$

Combined with Eq. (35), Eq. (36) is converted into

$$\frac{D_{CSH}}{D_{GP}} = \frac{1}{\mu_D}\phi_{CSH} = 0.059\phi_{CSH} + 0.226(\phi_{CSH})^{3.68} \quad (37)$$

Gel pores in C-S-H are generally of nano-meter size and D_{GP} is smaller than D_0 due to the increasing viscosity of pore solution in nanopores [59,60] and the surface effect, i.e. electrical double layer effect [61-63]. The average value of D_{GP} is normally regarded as around 10^{-10} m^2/s [60]. Thus, D_{GP} was set as 1.0×10^{-10} m^2/s in this study [48].

As indicated in Eq. (37), the ionic diffusivity of C-S-H is a function of gel porosity of C-S-H. The average gel porosity of C-S-H was found to be relatively stable in the same type of cement paste. Powers [64] indicated that the average gel porosity of C-S-H for Portland cement paste is around 0.3. Regarding fly ash blended cement paste, the gel porosity of C-S-H is lower than that for Portland cement paste [21,52]. Bentz [13] reported that the average gel porosity of C-S-H for fly ash blended cement paste is 0.2. As per these findings, in this work, the average gel porosities of C-S-H for Portland cement paste and fly ash blended cement paste were set as 0.3 and 0.2, respectively, and correspondingly the relative diffusivities of C-S-H to D_0 (i.e. $\frac{D_{CSH}}{D_0}$) for Portland cement paste and fly ash blended cement paste were calculated to be 0.00102 and 0.00062 using Eq. (37), which are close to those deduced using measured data of ionic diffusivity, i.e., 0.0025 for Portland cement paste [32] and 0.0005 for blended cement paste [65]. Accordingly, based on the relationship between relaxation time and ionic relative diffusivity (see benchmark tests in Section 3.1), the relaxation time of C-S-H for Portland and fly ash blended cement pastes is 0.50051 and 0.50031, respectively.

4. Experimental program

To determine the input parameters required for hydration model and validate the simulations, the characteristics of raw materials (e.g., particle size distribution, mineral phase content, and mineral phase distribution of binder particles), hydration process (e.g., released hydration heat, CH content, and degree of hydration of fly ash) and pore structure (e.g. porosity) of hydrated cement paste, and effective ionic diffusivity of hardened cement paste were measured.

4.1. Raw materials

The Portland cement used is Portland cement P.I. 52.5 (Chinese standard), similar to ASTM C150 Type I cement, the measured particle size distribution of which with a median diameter of 10.3 μm is shown in Fig. 5. The 28-d compressive strength of Portland cement paste with a water requirement of normal consistency of 0.274 is 59.6 MPa. Table 2 presents the main chemical composition and other physical properties of Portland cement, the estimated Bogue phase composition (volume fraction) of which is: 53.72% C_3S, 24.09% C_2S, 7.61% C_3A, 8.98% C_4AF and 5.6% $CaSO_4 \cdot 2H_2O$. Scanning electron microscopy (SEM) along with energy dispersive spectroscopy (EDS) was adopted to obtain the distribution of main mineral phases of cement particles. The detailed sample preparation and imaging process can be found in a previous publication [45]. Fig. 6 displays a segmented image of real cement powders at 800× magnification level. Based on imaging processing, the volume fractions of mineral phases can be calculated as 52.36% C_3S, 29.75% C_2S, 4.77% C_3A and 13.12% C_4AF, which are in consistence with the Bogue ones, suggesting that the segmented image is representative for the real Portland cement powder. In order to determine the distribution of mineral phases of cement powders, the autocorrelation function known to be a two-point correlation function was used [13], which is defined as the probability that two arbitrary points are in the same phase as the function of the distance between them. For an image with $M \times N$ pixel^2, the summation $S(x,y)$ can be calculated using the following equation:

$$S(x,y) = \sum_{i=1}^{M-x} \sum_{j=1}^{N-y} \frac{I(i,j) \times I(i+x,j+y)}{(M-x)(N-y)} \tag{38}$$

where $I(x,y)$ is 1 if the pixel at location (x,y) contains the phase of interest, otherwise $I(x,y)$ is 0.

$S(x,y)$ was then converted into the function of $S(r)$ for the distance r in pixels using bilinear interpolation on the $S(x,y)$ values as follows:

$$S(r) = \frac{1}{2r+1} \sum_{l=0}^{2r} S(r, \frac{\pi l}{4r}) \tag{39}$$

The calculated autocorrelation functions of silicate (C_3S+ C_2S), C_3S, and C_3A in Portland cement powders as inputs are shown in Fig. 7.

Regarding fly ash, a low-calcium fly ash produced in China was used, the chemical composition and physical properties of which are presented in Table 2. Fig. 5 shows the measured particle size distribution of fly ash, indicating that fly ash with a median diameter of 6.8 μm is much finer than

Portland cement. As mentioned in Section 2.2, the content of inert phases and amorphous phases of fly ash, i.e., CAS_2, S, and AS, are important inputs for the hydration model of fly ash blended cement. In order to quantify the content of mineral phases, the Rietveld refinement method with pure corundum as an internal standard was performed on the fly ash powders, which were carefully mixed with 10% pure corundum relative to the weight of fly ash powders and then examined by means of D8 discovery diffraction (Bruker Co, Germany). The X-ray diffraction (XRD) pattern was recorded ranging from 10° to 70° with the testing parameters of: 40 kV, 30 mA, Cu target Kα radiation, 0.3 s/step scanning speed and 0.02° step width. The quantitative XRD analysis was subsequently implemented using the software, X-Pert HighScore Plus. The composition was determined via Rietveld refinement using the fundamental parameter approach and the G-factor method [66]. The detailed XRD pattern of fly ash mixture is shown in Fig. 8. It can be observed that besides glass phases the fly ash powders are composed of quartz, mullite, maghemite and periclase. These crystalline phases are regarded as inert phases. The quantitative characterization indicates that fly ash is composed of 63% glass phase and 37% inert phase that consists of 23.1% quartz, 11.5% mullite and 2.3% periclase. In order to classify the glass phases of fly ash into basic phases (i.e., CAS_2, S and AS), the following assumptions were made: (1) Regarding the source of CaO, it is produced from $CaSO_4$ and glass CAS_2, and the content of $CaSO_4$ can be calculated based on the detectable content of SO_3. (2) The amorphous Al_2O_3 exists in CAS_2 and AS, and CAS_2 has the priority. (3) The remaining amorphous SiO_2 individually exists apart from that in AS and CAS_2. Based on these assumptions, the glass phases of fly ash can be grouped into 19.3% CAS_2, 22.4% S, 20.9% AS, and 0.4% $CaSO_4$. The content of different phases in fly ash is presented in Table 3.

Another input parameter of fly ash is the distribution of different phases on fly ash, which was measured following a similar procedure for obtaining the distribution of mineral phases on cement powders. Fig. 9 shows the backscattered electron (BSE) image, element mapping images, and Al-Si-Ca multispectral overlay image, which indicate that fly ash powders consist of the clusters of S, A-S and C-A-S, while most fly ash particles are composed of individual phases. Therefore, the fly ash particles are regarded as individual phases in the simulation.

4.2. Hydration and pore structure

The released hydration heat, CH content, degree of hydration of fly ash, and porosity of hardened cement paste were measured for validating the simulated hydration process and microstructure. In this study, cement pastes with w/b ratios of 0.3, 0.4 and 0.5, and 0, 10%, 30% and 50% replacement ratios of fly ash were investigated. Regarding the sample preparation of hardened cement paste, the cement powders were carefully mixed with fly ash and deionized water, and the mixtures were then cast into cylinder plastic containers with an inner diameter of 20 mm and height of 50 mm for microscopic characterization, followed by curing of specimens under standard curing conditions (20

± 2 °C, relative humidity > 95%).

4.2.1. Hydration heat

The hydration heat was measured using a TAM Air 8 channel isothermal calorimeter at 20 °C. Cement, fly ash and deionized water were weighted and equilibrated at 20±2 °C in an air-conditioned room. The cement pastes were evenly mixed for 2 min in a container. Approximate 10 g cement paste was poured into a plastic bottle that was then placed into the channel of the TAM Air isothermal calorimeter. The specific heat of cement paste (H_{paste}) can be calculated as:

$$H_{paste} = H_C x_C + H_{FA} x_{FA} + H_{water} x_{water} \quad (40)$$

where H_C, H_{FA} and H_{water} present the specific heat values of Portland cement, fly ash and water, x_C, x_{FA} and x_{water} denote the mass fractions of them. Herein, H_C = 0.76 J/(g·K), H_{FA} = 0.72 J/(g·K) and H_{water} = 4.18 J/(g·K) [67].

The data was automatically recorded using a computer program until 72 h. It should be noted that due to the disturbance of the signal resulted from the unbalance of temperature in the calorimeter, the first few minutes were not considered.

4.2.2. Degree of hydration of fly ash

The degree of hydration of fly ash in blended cement paste can be measured using BSE image processing techniques and selective dissolution method [17,42]. In this study, the selective dissolution method was used, which is based on the principle that fly ash in blended cement paste can react with CH to form acid-soluble hydration products, and the hydration products and unhydrated cement can dissolve in acid solution, leaving undissolved fly ash [68]. To dissolve hydration products and unhydrated cement for pure Portland cement and fly ash blended systems, different acids can be used, such as hydrochloric acid (HCl) [68], salicylic-acid + methanol [68], picric-acid + methanol [7], and HCl + salicylic-acid + methanol [69]. As the use of HCl has been included in the Chinese standard GB/T 12960-2007, it was adopted here following a similar procedure given in [70].

The entire experimental procedure includes: (1) The cement paste samples at various time points were crushed into small fragments. The coarse particles in the interior of samples were selected and immersed into isopropanol to stop hydration. The samples were soaked for 10 d and the solvent was changed three times during this process. (2) The fragments were grounded into finer particles using an agate mortar and were passed through a sieve with a 200-mesh size. The ground sample was stored in a vacuum drying oven for further analysis. One 150 ml beaker with 50 ml water was placed into the water bath on the electromagnetic stirrer in advance. The temperature was controlled at 20±2 °C. 0.5 g ground and sieved paste powder sample was added into the beaker and blended for 5 min to disperse homogeneously. (3) 40 ml HCl stored at 20±2 °C was added into the beaker and mixed for 25 min. The HCl was prepared using 1.95 g/ml concentrated HCl as the HCl-to-water volume ratio of 1:2. (4) The mixture was vacuum filtered on the pre-dried glass fibre filters and the residual

material was washed for 8 times using water and one time using ethanol. The whole process of washing and filtering was completed in 20 min. The filter paper and the dissolution residues were then transferred into a porcelain crucible. The crucible was ignited in an electric furnace at 300 °C, 450 °C and 950 °C, each for 1 h. The crucible was cooled down to room temperature and weighed. The degree of hydration of fly ash (α_{FA}) was determined by:

$$\alpha_{FA} = \frac{\frac{R_{FC}}{1-w_{NE}} - x_C R_C}{x_{FA} R_{FA}} \quad (41)$$

where R_{FC} is the residue per gram of fly ash blended cement paste, R_C and R_{FA} are the residue per gram of plain cement paste and the residue per gram of fly ash, and w_{NE} is the non-evaporable water content of fly ash blended cement paste.

4.2.3. Calcium hydroxide content

The CH content was determined through the thermal gravimetry analysis (TGA). Around 300 mg ground sample was weighed into alumina crucibles. The sample was heated at a step rate of 10 °C/min from room temperature to 105 °C and was kept at 105 °C for 30 min under N_2-purging in the TGA equipment. Afterwards, the sample was heated to 900 °C at the same heating rate. Since CH was decomposed between 400 °C and 550 °C, a sharp weight loss step can be observed. The tangential method [71] was used to determine the CH content (w_{CH}) that was calculated using the ignited weight of the cement paste sample.

$$w_{CH} = \frac{4.115 \Delta G_1}{\Delta G_0} \quad (42)$$

where ΔG_1 is the weight loss between 400 °C and 500 °C, and ΔG_0 is the remaining weight at 900 °C that is regarded as the weight of binder.

4.2.4. Porosity

The porosity in hardened cement paste was measured using mercury intrusion porosimetry (MIP). The measurement was performed with Micrometrics AutoPore IV 9500, for which the measuring range of pore sizes is between 3 nm and 360 μm. Before the MIP test, the crushed cement paste particles ranged from 1.25 to 2.5 mm for measurement were controlled by a square hole sieve and then dried at 60 °C for 48 h in a vacuum drying oven. Subsequently, the measurement was conducted in two stages: a manual low pressure running from 0.003 MPa to 0.21 MPa, and an automated high pressure running from 0.21 MPa to 242 MPa. The data was collected and addressed by a computer acting as a control module. After the low-pressure testing, the penetrometer was removed and weighted, followed by the high-pressure testing. MIP experiment was conducted with a 30 s pressure equilibration time and the contact angle was set as 130°.

4.3. Effective ionic diffusivity

To validate the simulated ionic diffusivity of hardened cement paste, the steady-state accelerated chloride diffusion tests as per NT build 355 were carried out. The experimental procedure refers to

that presented in [72]. Regarding sample preparation for chloride diffusion tests, the well-mixed cement paste specimens were cast in the 100-mm diameter and 300-mm high cylinders and demoulded after 24 h. The mixtures with w/b (w/c) ratios of 0.23, 0.35 and 0.53 for Portland cement paste and w/b ratio of 0.35 with fly ash replacement ratios of 10% 30% and 50% for fly ash blended cement paste were used. The samples were then cured under the standard curing conditions for 28, 60, and 120 d.

Before the test, the columned specimens (100 mm in diameter and 30 mm in height) were vacuum-saturated for 48 h, and the lateral surface was coated with epoxy. Subsequently, the specimen was placed between two upstream and downstream cells. Two mesh electrodes were placed on two sides of the specimen in such a way that the electrical field was applied primarily across the test specimen. One of the cells is called anode that was filled with 0.3 mol/L NaOH, while the other cell is called cathode that was filled with 3.0% NaCl. The cell was forced by a 30 V DC regulated power supply. During the test, the chloride ion concentration was determined from the solution in the anode cell, titrated with a 0.01 mol/L $AgNO_3$ solution. When the change of the cumulative chloride concentration reaches the steady state, the chloride diffusivity (D_{Cl}) in the specimen can be calculated as:

$$D_{Cl} = \frac{RKLV_d}{c_{up}FEA} \cdot \frac{\Delta c}{\Delta t} \tag{43}$$

where c_{up} is the chloride concentration in the upstream cell, E is the electrical field, R is the universal gas constant, F is the Faraday constant, K is the temperature, Δt is the interval time measured, V_d is the solution volume of downstream cell, Δc is the change of the chloride ion concentration, A is the surface area exposed to chloride ions, and L is the thickness of the specimen.

5. Validation and discussion

5.1. Hydration process and microstructural evolution

Based on the above-mentioned input parameters, the procedure for modelling hydration process and microstructural development including cement packing, phase segmentation, and hydration (see Fig. 1) was implemented. For cement packing, it should be mentioned that the spherical binder particles are represented in digital form and the radius of simulated binder particle is not continuous but the integral multiple of the resolution. As seen in Fig. 5, the simulated particle size distribution of Portland cement and fly ash shows good agreement with experimental data. In the simulation of hydration process, the microstructure of cement paste at any specific time point can be obtained. Taking fly ash blended cement paste with w/b ratio of 0.5 and 30% fly ash replacement ratio as an example, the 3D microstructure and pore structure at 0, 28 and 120 d are obtained and shown in Fig. 10. It is indicated that with the increase of curing age the binders are gradually consumed, and the corresponding hydration products produced fill the capillary pores, leading to the decrease in capillary porosity. Compared to the clinkers, the reaction rate of fly ash is much slower. As shown in Fig. 10,

the clinker particles cannot be distinguished in the paste at 28 d, while fly ash particles still clearly exist at 28 d, and some medium and large fly ash particles can even be found at 120 d. The low reaction rate for fly ash was also observed by Durdziński et al. [69], who reported that the experimental degree of hydration of fly ash is less than 30% even after 90 d of curing.

To quantitatively validate the simulations of hydration of fly ash blended cement, the simulated released heat, CH content, degree of hydration of fly ash and porosity in fly ash blended cement paste were compared with experimental data. Fig. 11 shows the simulated and experimental hydration heat of cement paste with w/b ratios of 0.3 and 0.5, and 0, 10%, 30%, and 50% replacement ratios. It is indicated that the simulated released heat in the early period (before 25 h) is higher than the measured heat. This can be explained by the fact that the early hydration process (e.g. induction period) is not explicitly considered in CEMHYD3D model due to lack of incorporation of hydration kinetics into the model [13] and the early cement hydration is still an open question. Moreover, the early hydration process of cement is determined by the small cement particles [47] but the particles smaller than the resolution cannot be well reflected in the model, which may lead to the larger dissolution probabilities of cement clinkers when fitting the experimental data. Therefore, the simulated hydration heat tends to be higher than the measured one, but it agrees well with the measured value after 30 h. Regarding the effect of fly ash on hydration heat, it can be found that the incorporation of fly ash significantly reduces the total released heat. As the fly ash replacement ratio increases, the reduction in total hydration heat within 72 h is more significant. For instance, the hydration heat of w/b = 0.3 fly ash blended cement with 50% fly ash is only 57% that of pure Portland cement paste.

Fig. 12 shows the simulated and experimental CH content in fly ash blended cement paste against curing age. The CH content increases dramatically in the early 3 d but tends to be stable and even slightly decreases with time in the paste with a high fly ash replacement ratio, which has a low CH content. For instance, 0.24 g/g binder is observed in the mature Portland cement paste by contrast to only 0.03 g/g binder in fly ash blended cement paste with 50% replacement ratio. This can be ascribed to the fact that the higher fly ash replacement ratio leads to the less CH produced in cement paste and more fly ash, in turn, needs more CH to react [4]. Overall, the simulated CH content shows good agreement with experimental data. The slight decreasing tendency for high fly ash replacement ratio, e.g. 50%, is also well simulated.

The simulated degree of hydration of fly ash against time together with experimental data is plotted in Fig. 13. The degree of hydration of fly ash increases with curing age, as demonstrated in Fig. 14 for the paste with w/b = 0.5 and 30% fly ash replacement ratio that the amorphous phases in fly ash are gradually consumed due to hydration. At the early curing age (e.g. 7 d), the degree of hydration of fly ash is low and only the surface of fly ash is consumed. By contrast, at the later curing age (e.g. 90 d), the quick consumption of the small and medium fly ash particles occurs, but the large

particles can still be identified. The higher fly ash replacement ratio of paste results in a lower degree of hydration of fly ash. For example, the degree of hydration of fly ash in paste with 10% fly ash replacement ratio is about 33% higher than that with 50% fly ash replacement ratio at 90 d. This can be attributed to the lower activated ability of pore solution with lower pH and concentration of Ca^{2+} as a consequence of the higher fly ash replacement ratio [7]. Overall, the simulated and experimental degrees of hydration of fly ash are in good agreement.

Regarding porosity of fly ash blended cement paste, the simulated and measured values of cement pastes with 50% replacement ratio are shown in Fig. 15. Herein, the simulated porosities of cement paste include capillary porosity, gel porosity and total porosity. Based on the assumed gel porosity of C-S-H, i.e., 0.3 for Portland cement paste and 0.2 for fly ash blended cement paste, the simulated total porosity (ϕ_t) can be calculated as:

$$\phi_t = \phi_{CP} + \varphi_{CSH}\phi_{CSH} \quad (44)$$

where ϕ_{CP} and φ_{CSH} are the volume fractions of capillary pores and C-S-H in cement paste.

It can be observed that the capillary porosity of fly ash blended cement paste dramatically decreases in the first few days and then tends to be stable. On contrary, the gel porosity of paste shows an opposite changing tendency, i.e. a significant increase at the early stage and becoming stable after that. The evolution of capillary porosity and gel porosity with curing age corresponds to the formation process of solid skeleton as a result of hydration with time [9]. In cement paste, the gel porosity is much smaller than capillary porosity and thus the total porosity shows a similar changing trend to capillary porosity. It can be also found that the capillary porosity of paste is strongly affected by w/b ratio, while the gel porosity of paste is not sensitive to w/b ratio. However, the contribution of the gel porosity to the total porosity is increased with decreasing w/b ratio. For example, as the w/b ratio reduces from 0.5 to 0.3, the volume fraction of gel pores in total porosity increases from 16.8% to 34.1%. It is worth mentioning that it is difficult to experimentally distinguish the capillary porosity and gel porosity, as there is still no uniform criterion for distinguishing pore space in cement paste [73]. In this study, the porosity measured by MIP was regarded as the total porosity, including capillary porosity and gel porosity. As seen in Fig. 15, the simulated total porosity and measured data are in good agreement.

5.2. Effective ionic diffusivity

After obtaining the virtual 3D microstructures of fly ash blended cement paste, the microstructure-based modelling of ionic diffusivity using LB diffusion model was carried out. The contribution of different phases in cement paste, i.e. capillary pores and porous C-S-H gels, to the overall ionic diffusion was estimated. In addition, the effects of various factors including curing age, fly ash replacement ratio and w/b ratio on ionic diffusivity of cement paste were investigated, which were validated using experimental results. Finally, the relationship between ionic diffusivity and pore

structure characteristics of fly ash blended cement was studied in a quantitative manner.

5.2.1. Contribution of capillary pore and C-S-H gel to overall ionic diffusion

In the microstructure of fly ash blended cement paste, both capillary pore and porous C-S-H can contribute to ionic diffusion and D_0 is much higher than D_{CSH}. To evaluate the contribution of C-S-H to the total ionic diffusion, the fly ash blended cement paste was regarded as a composite material of capillary pores and solid phases, and capillary pores, porous C-S-H gel and other solid phases, respectively. Here, fly ash blended cement pastes with w/b of 0.5 and fly ash replacement ratios of 0% and 20% at 120 d were investigated and compared. Fig. 16 shows the steady-state concentration distribution of ions in capillary pore network and whole microstructure including capillary pore and C-S-H of cement pastes. It can be observed that the diffusion paths for considering only capillary pores are obviously less compared to that for considering both capillary pores and gel pores in C-S-H. The simulated ionic diffusivity values for reference cement paste without fly ash are 9.8×10^{-13} m^2/s and 5.5×10^{-12} m^2/s respectively if considering only capillary pores and both capillary pores and C-S-H, while for cement paste with 20% fly ash replacement ratio they are found to be 1.04×10^{-12} m^2/s and 4.22×10^{-12} m^2/s. These indicate that the predicted ionic diffusivity considering the contribution of C-S-H is 4-6 times that only considering the ionic diffusion through capillary pores in cement paste and neglecting the contribution of gel pores in C-S-H. This can be ascribed to the fact that part of capillary pores are isolated or dead-ended which are not effective channels for ionic diffusion [62]. For example, the volume fractions of connected capillary pore in virtual cement pastes with fly ash replacement ratios of 0% and 20% calculated using the burning algorithm [46] are only 0.44 and 0.40, respectively. As the capillary porosity decreases, the connectivity of capillary pore network significantly decreases and capillary porosity depercolation would occur [74]. However, because of gel pores in C-S-H, the isolated or dead-ended capillary pores can become connected with the other part of capillary pores by C-S-H. Although the ionic diffusivity in C-S-H is much smaller than that in capillary pore, C-S-H has a significant contribution to the increase in connectivity of pore network and thus to the ionic diffusivity in cement paste, which is consistent with the findings reported in [33]. In addition, the ionic diffusivity through capillary pore only for the paste without fly ash is larger than that with the fly ash replacement ratio of 20%, while the ionic diffusivity through microstructure (i.e. capillary pore along with C-S-H) is opposite, which implies that the incorporation of fly ash results in an increase in the ionic diffusivity through capillary pores only but a significant decrease in the ionic diffusivity in paste due to the produced C-S-H by pozzolanic reaction of fly ash.

5.2.2. Validation of ionic diffusivity

Fig. 17 shows a comparison of the simulated and measured ionic diffusivity of fly ash blended cement pastes with w/b ratio of 0.35 and fly ash replacement ratios of 0%, 10%, 30% and 50% against curing age. The ionic diffusivity of cement pastes decreases from 10^{-10} m^2/s to 10^{-13} m^2/s with increasing

curing age from 1 d to 365 d. In the early period (before 28 d), there is a sharp reduction in ionic diffusivity due to the hydration process of Portland cement. With the increase of fly ash replacement ratio, this reduction trend is extended further to several tens of days or even a few hundred days (see Fig. 16c and d), which can be attributed to the pozzolanic effect of fly ash with a lower reaction rate that plays an important role in the later stage of hydration of blended system. In LB simulations, the natural ionic diffusion was studied, while the experimental data were obtained from steady-state accelerated chloride diffusion tests, which were found to be 1.5 to 6 times that measured by natural diffusion cell tests, depending on the difference in ion concentration between upstream and downstream [75]. In this study, the chloride concentration difference used is 0.53 mol/L and the corresponding contrast ratio is approximately 2 [75]. Accordingly, the measured ionic diffusivity of cement pastes with and without fly ash through steady-state accelerated chloride diffusion tests is shown in Fig. 17 as well for comparison, which indicates a good agreement between LB simulation results and experimental data.

To further investigate the effect of w/b ratio, the ionic diffusivity of fly ash cement pastes with six replacement ratios, i.e., 0%, 10%, 20%, 30%, 40% and 50%, was simulated, the results of which are compared with the experimental data obtained from literature [25, 28, 76-79], as shown in Fig. 18. The details of tests and specimens used in the literature were summarized in Table 4. It can be observed that the simulated ionic diffusivity increases with the increase of w/b ratio for all cement pastes with various fly ash replacement ratios. In addition, the incorporation of fly ash affects the ionic diffusivity of cement paste but this effect is dependent on the replacement ratio and w/b ratio. When the fly ash replacement ratio is no higher than 30%, the addition of fly ash can help to decrease the ionic diffusivity of cement paste even at w/b = 0.6. For the higher replacement ratio, i.e., 40% and 50%, the ionic diffusivity of fly ash blended cement paste is higher than that of cement paste without fly ash, except for w/b ratio less than 0.3. The LB simulation results agree well with experimental data, particularly for cement pastes with replacement ratios of 0-30% and 50%. However, the discrepancy between simulated and experimental data is increased with increasing w/b ratio for cement paste with fly ash replacement ratio of 40%. This can be ascribed to the difference in raw materials used in this study and the experiments by Ampadu et al. [25], which would affect the microstructure as well as the ionic diffusivity of fly ash blended cement paste [7].

5.2.3. Relationship between ionic diffusivity and pore structure

To better understand the effect of fly ash on ionic diffusivity of cement paste, it is necessary to correlate the ionic diffusivity with pore structure of fly ash blended cement paste. Taking the fly ash blended cement pastes with w/b = 0.4 and replacement ratios of 0%, 10%, 30% and 50% as examples, the ionic diffusivity as a function of capillary porosity is displayed in Fig. 19. There does not exist a unique relationship between ionic diffusivity and capillary porosity for fly ash blended cement pastes

with various replacement ratios. It is different from the finding for pure Portland cement paste that the ionic diffusivity of Portland cement paste against capillary porosity follows an exponential relationship, independent on w/b ratio [80], but is consistent with the finding by Nokken and Hooton [26] that although an exponential equation can be used to describe the relationship between ionic diffusivity and capillary porosity, the constants in the exponential equation for different fly ash blended cement pastes vary over a wide range. This implies that compared to Portland cement paste the pore space accessible for diffusion and the connectivity of capillary porosity are dramatically changed with fly ash replacement ratio, which are discussed in detail below.

It can be seen from Fig. 19 that when the capillary porosity is higher than 0.2 the ionic diffusivity against capillary porosity for cement pastes with different fly ash content is close to each other and shows a similar increasing trend. However, the ionic diffusivity of cement pastes containing fly ash at the capillary porosity values of lower than 0.2 tends to be smaller than that of pure Portland cement paste, which can be attributed to the depercolation of capillary porosity [74]. Before depercolation of capillary porosity occurs, the capillary pores are the dominant diffusion paths in cement paste. However, after depercolation of capillary porosity, the gel pores in C-S-H play a key role in ionic diffusion through cement paste, as illustrated in Fig. 16, although the ionic diffusivity in C-S-H is much smaller than that in capillary pore. Since the ionic diffusivity in pozzolanic C-S-H gels in cement paste with fly ash is yet smaller than that in C-S-H gels produced in pure Portland cement paste, fly ash blended cement paste exhibits a smaller effective ionic diffusivity compared to cement paste without fly ash after capillary porosity depercolation.

In order to further estimate the effect of capillary porosity depercolation on ionic diffusivity of fly ash blended cement paste, the connectivity of capillary pores against capillary porosity was obtained and plotted in Fig. 19, which indicates a capillary porosity depercolation threshold around 0.2 capillary porosity in all cement pastes. This is consistent with the value reported in [81] based on image-based Portland cement paste with a resolution of 1 μm/voxel. The connectivity of capillary pores of cement paste as a function of capillary porosity slightly increases with increasing fly ash content and follows a similar changing trend until the depercolation threshold of capillary porosity (i.e. 0.2), suggesting that the incorporation of fly ash has no significant effect on the capillary pore structure of fly ash blended cement paste and the decrease in ionic diffusivity of fly ash blended cement paste is not ascribed to the change of capillary porosity and connectivity of capillary pore. This aspect can be further confirmed by the relationship between ionic diffusivity and accessible capillary porosity (i.e. capillary porosity multiplied by connectivity of capillary pores), as shown in Fig. 20, which indicates a perfect linear relationship between the logarithmic value of ionic diffusivity and the accessible capillary porosity of cement paste regardless of fly ash replacement ratio, before the percolation of capillary pores occurs (i.e. accessible capillary porosity > 0). However, after

capillary porosity depercolation (i.e. accessible capillary porosity = 0), the fly ash replacement ratio has a significant influence on ionic diffusivity of cement paste (see Figs. 19 and 20), where the gel pores in C-S-H gels act as the dominant diffusion paths. This further suggests that after capillary porosity depercolation the difference in ionic diffusivity of fly ash blended cement paste is a result of the difference in ionic diffusivity in the pozzolanic C-S-H gels due to different volume fractions gel pores and different tortuosity of gel pores in C-S-H gels.

6. Conclusions

In this paper, an integrated modelling framework consisting of hydration model and lattice Boltzmann diffusion model is presented to investigate the 3D microstructure and ionic diffusivity of fly ash blended cement paste. Firstly, a voxel-based hydration model of fly ash blended cement is developed to simulate the hydration process and microstructural development considering different factors including types of fly ash, temperature and pH of pore solution, which is validated with experimental data. Subsequently, a lattice Boltzmann model for diffusion is developed taking into consideration of the contributions of both capillary pores and gel pores in C-S-H gels to overall ionic diffusion through cement paste. Finally, the effects of various factors including curing age, fly ash replacement ratio and w/b ratio on ionic diffusivity of fly ash blended cement paste are estimated. Based on the findings of this study, the following conclusions can be drawn:

- The backscattered electron image and element mapping images indicate that fly ash is comprised of the clusters of S, A-S and C-A-S, while most fly ash particles consist of the individual phases.
- The simulated hydration process and pore structure of fly ash blended cement system using the developed hydration model agree well with experimental data in terms of hydration heat, calcium hydroxide content, degree of hydration of fly ash, and porosity.The experimental and simulated results both indicate that the hydration process and pore structure of fly ash blended cement system are highly associated with w/b ratio, fly ash replacement rato, and curing age.
- The simulation results show that the contribution of C-S-H to overall ionic diffusion through cement paste cannot be ignored since the isolated or dead-ended capillary pores can be connected by the gel pores in C-S-H gels in cement paste. The ionic diffusivity of cement paste with w/b = 0.5 considering the contribution of C-S-H gels is 4-6 times that only accounting for the ionic diffusion through capillary pore in cement paste and neglecting the contribution of C-S-H gels.
- As observed in experiments and simulations that there is a sharp reduction in ioinc diffusivity before 28 d due to the hydration process of Portland cement. With the increase of fly ash replacement ratio, this reduction trend is extended further to several tens of days or even a few hundred days, which can be attributed to the pozzolanic effect of fly ash with a lower reaction rate that plays an important role in the later stage of hydration of blended cement system.
- The effect of fly ash on ionic diffusivity of fly ash blended cement paste is associated with the fly

ash replacement ratio and w/b ratio. The addition of fly ash up to 30% as a partial replacement of cement can help reduce the ionic diffusivity of cement paste, while the further increase of fly ash replacement level results in a higher ionic diffusivity of blended cement paste compared to reference Portland cement paste specimen, except for the specimens with w/c ratio lower than 0.3.

- There exists a perfect linear relationship between the ionic diffusivity of fly ash blended cement paste and the accessible capillary porosity before depercolation of capillary pores. After the depercolation of capillary pores occurs, the effect of fly ash on ionic diffusivity of blended cement paste becomes more significant and the reduction in ionic diffusivity of fly ash blended cement paste with the increase of fly ash content can be attributed to lower ionic diffusivity in the pozzolanic C-S-H gels compared to normal C-S-H gels in Portland cement paste.

Acknowledgments

The authors gratefully acknowledge the financial support from the Engineering and Physical Sciences Research Council, United Kingdom (EP/R041504/1 and EP/N509577/1, project reference: 1836739) as well as the National Key Research and Development Program of China (2017YFB0310001) and the State Key Laboratory of Silicate Materials for Architectures (Wuhan University of Technology), China (SYSJJ2018-08). The financial support provided by University College London (UCL) and China Scholarship Council (CSC) to the first author is also gratefully acknowledged. The authors would like to thank Dr. Zhiyong Liu, Mr. Rusheng Qian and Mr. Jiashun Shi from Southeast University, China for their help with experiments.

References

[1] D.P. Bentz, C.F. Ferraris, M.A. Galler, A.S. Hansen, J.M. Guynn, Influence of particle size distributions on yield stress and viscosity of cement–fly ash pastes, Cement and Concrete Research 42(2) (2012) 404-409.

[2] M. Şahmaran, İ.Ö. Yaman, M. Tokyay, Transport and mechanical properties of self consolidating concrete with high volume fly ash, Cement and Concrete Composites 31(2) (2009) 99-106.

[3] P. Van den Heede, E. Gruyaert, N. De Belie, Transport properties of high-volume fly ash concrete: Capillary water sorption, water sorption under vacuum and gas permeability, Cement and Concrete Composites 32(10) (2010) 749-756.

[4] Q. Zeng, K. Li, T. Fen-chong, P. Dangla, Determination of cement hydration and pozzolanic reaction extents for fly-ash cement pastes, Construction and Building Materials 27(1) (2012) 560-569.

[5] M. Cyr, P. Lawrence, E. Ringot, Efficiency of mineral admixtures in mortars: quantification of the physical and chemical effects of fine admixtures in relation with compressive strength, Cement and Concrete Research 36(2) (2006) 264-277.

[6] A. Xu, S. Sarkar, L.-O. Nilsson, Effect of fly ash on the microstructure of cement mortar, Materials

and Structures 26(7) (1993) 414-424.
[7] L. Lam, Y. Wong, C. Poon, Degree of hydration and gel/space ratio of high-volume fly ash/cement systems, Cement and Concrete Research 30(5) (2000) 747-756.
[8] E. Berry, R. Hemmings, B. Cornelius, Mechanisms of hydration reactions in high volume fly ash pastes and mortars, Cement and Concrete Composites 12(4) (1990) 253-261.
[9] Q. Zeng, K. Li, T. Fen-Chong, P. Dangla, Pore structure characterization of cement pastes blended with high-volume fly-ash, Cement and Concrete Research 42(1) (2012) 194-204.
[10] S. Lu, E. Landis, D. Keane, X-ray microtomographic studies of pore structure and permeability in Portland cement concrete, Materials and Structures 39(6) (2006) 611-620.
[11] M. Yio, H. Wong, N. Buenfeld, Representative elementary volume (REV) of cementitious materials from three-dimensional pore structure analysis, Cement and Concrete Research 102 (2017) 187-202.
[12] F. Luzzati, A. Fasolo, P. Peretto, Combining confocal laser scanning microscopy with serial section reconstruction in the study of adult neurogenesis, Frontiers in neuroscience 5 (2011) 70.
[13] D.P. Bentz, CEMHYD3D: A three-dimensional cement hydration and microstructure development modelling package. Version 2.0, US Department of Commerce, National Institute of Standards and Technology 2000.
[14] K. Van Breugel, Numerical simulation of hydration and microstructural development in hardening cement-based materials (I) theory, Cement and Concrete Research 25(2) (1995) 319-331.
[15] S. Bishnoi, K.L. Scrivener, μic: A new platform for modelling the hydration of cements, Cement and Concrete Research 39(4) (2009) 266-274.
[16] K. Maekawa, T. Ishida, T. Kishi, Multi-scale modeling of concrete performance, Journal of Advanced Concrete Technology 1(2) (2003) 91-126.
[17] D.P. Bentz, S. Remond, Incorporation of fly ash into a 3-D cement hydration microstructure model, US Department of Commerce, Technology Administration, National Institute of Standards and Technology 1997.
[18] N. Robeyst, C.U. Grosse, N. De Belie, Relating ultrasonic measurements on fresh concrete with mineral additions to the microstructure development simulated by Cemhyd3D, Cement and Concrete Composites 33(6) (2011) 680-693.
[19] P. Gao, Simulation of hydration and microstructure development of blended cements, PhD thesis, Delft University of Technology, 2018.
[20] S. Bishnoi, S. Joseph, A. Kaur, Microstructural modelling of the strength of mortars containing fly ash using μic, Construction and Building Materials 163 (2018) 912-920.
[21] X.Y. Wang, H.S. Lee, Modeling the hydration of concrete incorporating fly ash or slag, Cement and Concrete Research 40(7) (2010) 984-996.

[22] B. Violetta, Life-365 service life prediction model, Concrete International 24(12) (2002) 53-57.
[23] R.A. Patel, Q.T. Phung, S.C. Seetharam, J. Perko, D. Jacques, N. Maes, G. De Schutter, G. Ye, K. Van Breugel, Diffusivity of saturated ordinary Portland cement-based materials: A critical review of experimental and analytical modelling approaches, Cement and Concrete Research 90 (2016) 52-72.
[24] L. Tang, H. Sørensen, Precision of the Nordic test methods for measuring the chloride diffusion/migration coefficients of concrete, Materials and Structures 34(8) (2001) 479.
[25] K. Ampadu, K. Torii, M. Kawamura, Beneficial effect of fly ash on chloride diffusivity of hardened cement paste, Cement and Concrete Research 29(4) (1999) 585-590.
[26] M. Nokken, R. Hooton, Using pore parameters to estimate permeability or conductivity of concrete, Materials and Structures 41(1) (2008) 1.
[27] B.H. Oh, S.Y. Jang, Prediction of diffusivity of concrete based on simple analytic equations, Cement and Concrete Research 34(3) (2004) 463-480.
[28] H. Zhou, X.-Z. Zhou, J. Zhang, J.-J. Zheng, Effective Medium Method for Chloride Diffusion Coefficient of Mature Fly Ash Cement Paste, Materials 12(5) (2019) 811.
[29] C.F. Dunant, B. Bary, A.B. Giorla, C. Péniguel, J. Sanahuja, C. Toulemonde, A.-B. Tran, F. Willot, J. Yvonnet, A critical comparison of several numerical methods for computing effective properties of highly heterogeneous materials, Advances in Engineering Software 58 (2013) 1-12.
[30] M.I. Idiart, F. Willot, Y.-P. Pellegrini, P.P. Castaneda, Infinite-contrast periodic composites with strongly nonlinear behavior: Effective-medium theory versus full-field simulations, International Journal of Solids and Structures 46(18) (2009) 3365-3382.
[31] S. Das, A. Maroli, S.S. Singh, T. Stannard, X. Xiao, N. Chawla, N. Neithalath, A microstructure-guided constitutive modeling approach for random heterogeneous materials: Application to structural binders, Computational Materials Science 119 (2016) 52-64.
[32] E. Garboczi, D. Bentz, Computer simulation of the diffusivity of cement-based materials, Journal of Materials Science 27(8) (1992) 2083-2092.
[33] M. Zhang, G. Ye, K. Van Breugel, Microstructure-based modeling of water diffusivity in cement paste, Construction and Building Materials 25(4) (2011) 2046-2052.
[34] M. Zhang, G. Ye, K. van Breugel, Modeling of ionic diffusivity in non-saturated cement-based materials using lattice Boltzmann method, Cement and Concrete Research 42(11) (2012) 1524-1533.
[35] L. Liu, W. Sun, G. Ye, H. Chen, Z. Qian, Estimation of the ionic diffusivity of virtual cement paste by random walk algorithm, Construction and Building Materials 28(1) (2012) 405-413.
[36] N. Ukrainczyk, E. Koenders, Representative elementary volumes for 3D modeling of mass transport in cementitious materials, Modelling and Simulation in Materials Science and Engineering 22(3) (2014) 035001.

[37] J.F. Young, W. Hansen, Volume relationships for CSH formation based on hydration stoichiometries, MRS Online Proceedings Library Archive 85 (1986).
[38] D.P. Bentz, Three-dimensional computer simulation of Portland cement hydration and microstructure development, Journal of the American Ceramic Society 80(1) (1997) 3-21.
[39] R. Helmuth, Fly ash in cement and concrete, 1987.
[40] V.G. Papadakis, Effect of fly ash on Portland cement systems: Part I. Low-calcium fly ash, Cement and Concrete Research 29(11) (1999) 1727-1736.
[41] T. Wang, T. Ishida, Multiphase pozzolanic reaction model of low-calcium fly ash in cement systems, Cement and Concrete Research 122 (2019) 274-287.
[42] S. Rémond, D. Bentz, P. Pimienta, Effects of the incorporation of municipal solid waste incineration fly ash in cement pastes and mortars: II: modeling, Cement and Concrete Research 32(4) (2002) 565-576.
[43] Z. Tan, Experimental study and numerical simulation of hydration and microstructure development of ternary cement-based materials, PhD thesis, Ghent University, 2015.
[44] Y. Gao, G. De Schutter, G. Ye, Z. Tan, K. Wu, The ITZ microstructure, thickness and porosity in blended cementitious composite: Effects of curing age, water to binder ratio and aggregate content, Composites Part B: Engineering 60 (2014) 1-13.
[45] C. Liu, R. Huang, Y. Zhang, Z. Liu, M. Zhang, Modelling of irregular-shaped cement particles and microstructural development of Portland cement, Construction and Building Materials 168 (2018) 362-378.
[46] C. Liu, G. Liu, Z. Liu, L. Yang, M. Zhang, Y. Zhang, Numerical simulation of the effect of cement particle shapes on capillary pore structures in hardened cement pastes, Construction and Building Materials 173 (2018) 615-628.
[47] J.W. Bullard, E.J. Garboczi, A model investigation of the influence of particle shape on portland cement hydration, Cement and Concrete Research 36(6) (2006) 1007-1015.
[48] C. Liu, C. Qian, R. Qian, Z. Liu, H. Qiao, Y. Zhang, Numerical prediction of effective diffusivity in hardened cement paste between aggregates using different shapes of cement powder, Construction and Building Materials 223 (2019) 806-816..
[49] R.T. Chancey, P. Stutzman, M.C. Juenger, D.W. Fowler, Comprehensive phase characterization of crystalline and amorphous phases of a Class F fly ash, Cement and Concrete Research 40(1) (2010) 146-156.
[50] P.T. Durdziński, C.F. Dunant, M.B. Haha, K.L. Scrivener, A new quantification method based on SEM-EDS to assess fly ash composition and study the reaction of its individual components in hydrating cement paste, Cement and Concrete Research 73 (2015) 111-122.
[51] W. Chen, Hydration of slag cement-Theory, modelling and application, PhD Thesis, University

of Twente, 2007.
[52] K. Maekawa, T. Ishida, T. Kishi, Multi-scale modeling of structural concrete, CRC Press 2014.
[53] N. Jeong, D.H. Choi, C.L. Lin, Estimation of thermal and mass diffusivity in a porous medium of complex structure using a lattice Boltzmann method, International Journal of Heat and Mass Transfer 51(15-16) (2008) 3913-3923.
[54] M. Wang, J. Wang, N. Pan, S. Chen, Mesoscopic predictions of the effective thermal conductivity for microscale random porous media, Physical Review E 75(3) (2007) 036702.
[55] Y. Xuan, K. Zhao, Q. Li, Investigation on mass diffusion process in porous media based on Lattice Boltzmann method, International Journal of Heat and Mass Transfer 46(10) (2010) 1039-1051.
[56] R.A. Robinson, Stokes, RH Electrolyte Solutions, London, Butterworths Scientific Publications 19550(2) (1959) 540-4.
[57] H.M. Jennings, A model for the microstructure of calcium silicate hydrate in cement paste, Cement and Concrete Research 30(1) (2000) 101-116.
[58] H. Ma, D. Hou, Z. Li, Two-scale modeling of transport properties of cement paste: Formation factor, electrical conductivity and chloride diffusivity, Computational Materials Science 110 (2015) 270-280.
[59] Y. Ichikawa, K. Kawamura, N. Fujii, T. Nattavut, Molecular dynamics and multiscale homogenization analysis of seepage/diffusion problem in bentonite clay, International Journal for Numerical Methods in Engineering 54(12) (2002) 1717-1749.
[60] P. Pivonka, C. Hellmich, D. Smith, Microscopic effects on chloride diffusivity of cement pastes—a scale-transition analysis, Cement and Concrete Research 34(12) (2004) 2251-2260.
[61] Y. Zhang, C. Liu, Z. Liu, G. Liu, L. Yang, Modelling of diffusion behavior of ions in low-density and high-density calcium silicate hydrate, Construction and Building Materials 155 (2017) 965-980.
[62] Y. Yang, R.A. Patel, S.V. Churakov, N.I. Prasianakis, G. Kosakowski, M. Wang, Multiscale modeling of ion diffusion in cement paste: electrical double layer effects, Cement and Concrete Composites 96 (2019) 55-65.
[63] D. Hou, Z. Li, Molecular dynamics study of water and ions transport in nano-pore of layered structure: A case study of tobermorite, Microporous and Mesoporous Materials 195 (2014) 9-20.
[64] T.C. Powers, Structure and physical properties of hardened Portland cement paste, Journal of the American Ceramic Society 41(1) (1958) 1-6.
[65] D.P. Bentz, Influence of silica fume on diffusivity in cement-based materials: II. Multi-scale modeling of concrete diffusivity, Cement and Concrete Research 30(7) (2000) 1121-1129.
[66] D. Jansen, F. Goetz-Neunhoeffer, B. Lothenbach, J. Neubauer, The early hydration of Ordinary Portland Cement (OPC): An approach comparing measured heat flow with calculated heat flow from QXRD, Cement and Concrete Research 42(1) (2012) 134-138.

[67] P. Choktaweekarn, W. Saengsoy, S. Tangtermsirikul, A model for predicting the specific heat capacity of fly-ash concrete, ScienceAsia 35(2) (2009) 178-182.
[68] S. Ohsawa, K. Asaga, S. Goto, M. Daimon, Quantitative determination of fly ash in the hydrated fly ash-$CaSO_4 \cdot 2H_2O$ Ca (OH) $_2$ system, Cement and Concrete Research 15(2) (1985) 357-366.
[69] P.T. Durdziński, M. Ben Haha, S.A. Bernal, N. De Belie, E. Gruyaert, B. Lothenbach, E. Menéndez Méndez, J.L. Provis, A. Schöler, C. Stabler, Z. Tan, Y. Villagrán Zaccardi, A. Vollpracht, F. Winnefeld, M. Zając, K.L. Scrivener, Outcomes of the RILEM round robin on degree of reaction of slag and fly ash in blended cements, Materials and Structures 50(2) (2017).
[70] F. Han, J. Liu, P. Yan, Comparative study of reaction degree of mineral admixture by selective dissolution and image analysis, Construction and Building Materials 114 (2016) 946-955.
[71] K.D. Weerdt, E. Sellevold, K.O. Kjellsen, H. Justnes, Fly ash–limestone ternary cements: effect of component fineness, Advances in Cement Research 23(4) (2011) 203-214.
[72] G. Sun, Y. Zhang, W. Sun, Z. Liu, C. Wang, Multi-scale prediction of the effective chloride diffusion coefficient of concrete, Construction and Building Materials 25(10) (2011) 3820-3831.
[73] H.M. Jennings, J.W. Bullard, J.J. Thomas, J.E. Andrade, J.J. Chen, G.W. Scherer, Characterization and modeling of pores and surfaces in cement paste, Journal of Advanced Concrete Technology 6(1) (2008) 5-29.
[74] Z. Liu, Y. Zhang, Q. Jiang, W. Zhang, J. Wu, Solid phases percolation and capillary pores depercolation in hydrating cement pastes, Journal of Materials in Civil Engineering 26(12) (2013) 04014090.
[75] M. Castellote, C. Andrade, C. Alonso, Measurement of the steady and non-steady-state chloride diffusion coefficients in a migration test by means of monitoring the conductivity in the anolyte chamber. Comparison with natural diffusion tests, Cement and Concrete Research 31(10) (2001) 1411-1420.
[76] C. Page, N. Short, A. El Tarras, Diffusion of chloride ions in hardened cement pastes, Cement and Concrete Research 11(3) (1981) 395-406.
[77] S. Goto, D.M. Roy, Diffusion of ions through hardened cement pastes, Cement and Concrete Research 11(5-6) (1981) 751-757.
[78] S. Yu, C. Page, Diffusion in cementitious materials: 1. Comparative study of chloride and oxygen diffusion in hydrated cement pastes, Cement and Concrete Research 21(4) (1991) 581-588.
[79] L. Tang, L.O. Nilsson, Chloride diffusivity in high strength concrete at different ages, Nordic Concrete Research 11(1) (1992) 162-171.
[80] M. Zhang, G. Ye, K. van Breugel, Multiscale lattice Boltzmann-finite element modelling of chloride diffusivity in cementitious materials. Part II: Simulation results and validation, Mechanics Research Communications 58 (2014) 64-72.

[81] G. Sant, D. Bentz, J. Weiss, Capillary porosity depercolation in cement-based materials: Measurement techniques and factors which influence their interpretation, Cement and Concrete Research 41(8) (2011) 854-864.

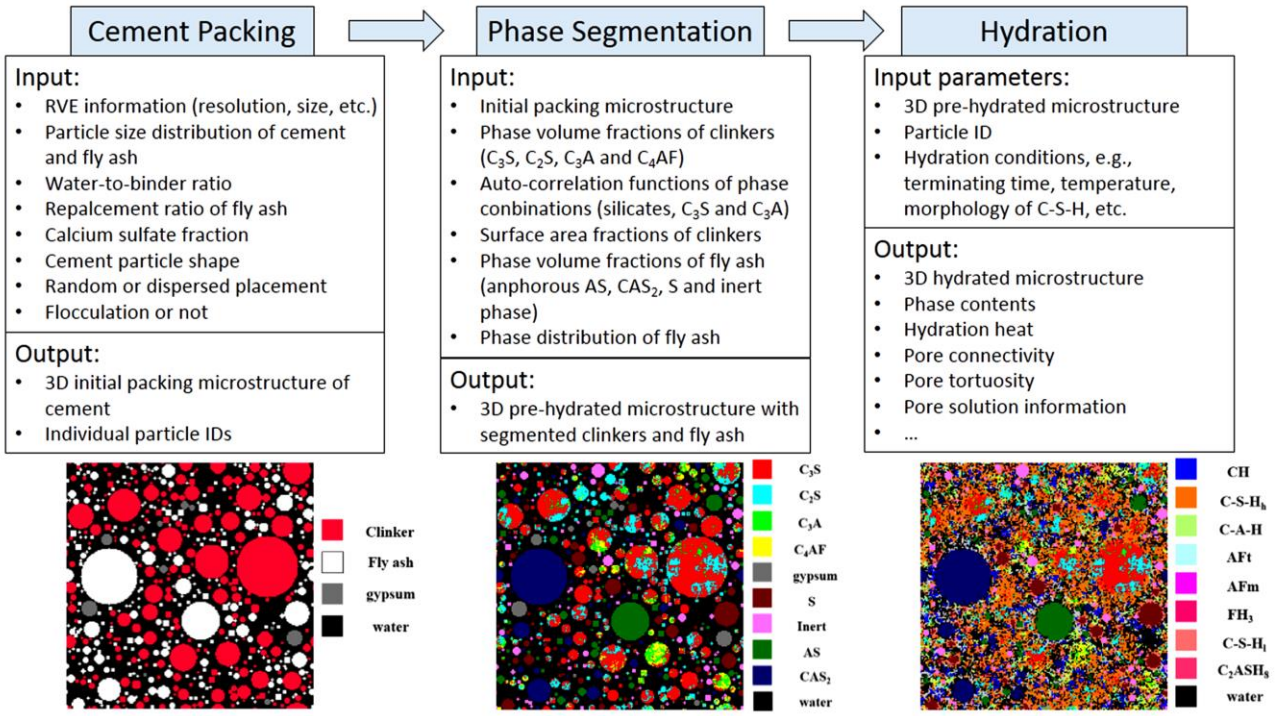

Fig. 1. Flowchart for the generation of hydrated fly ash blended cement paste.

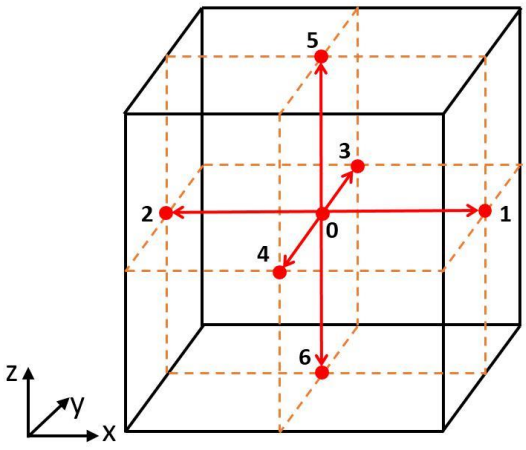

Fig. 2. D3Q7 cubic lattice model.

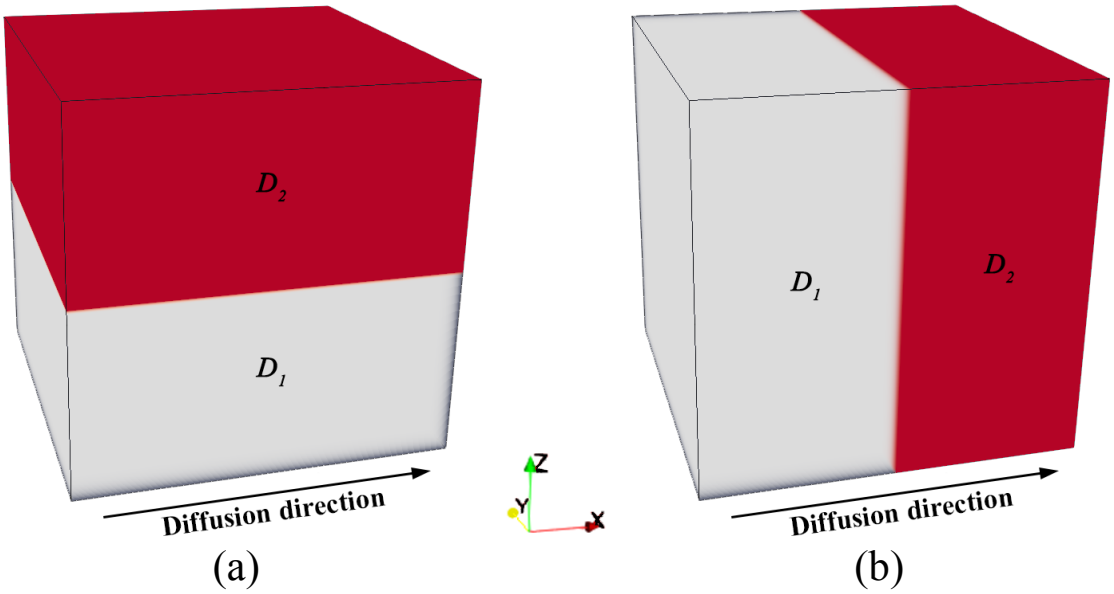

Fig. 3. Basic structure of dual-component medium: (a) parallel mode, and (b) series mode.

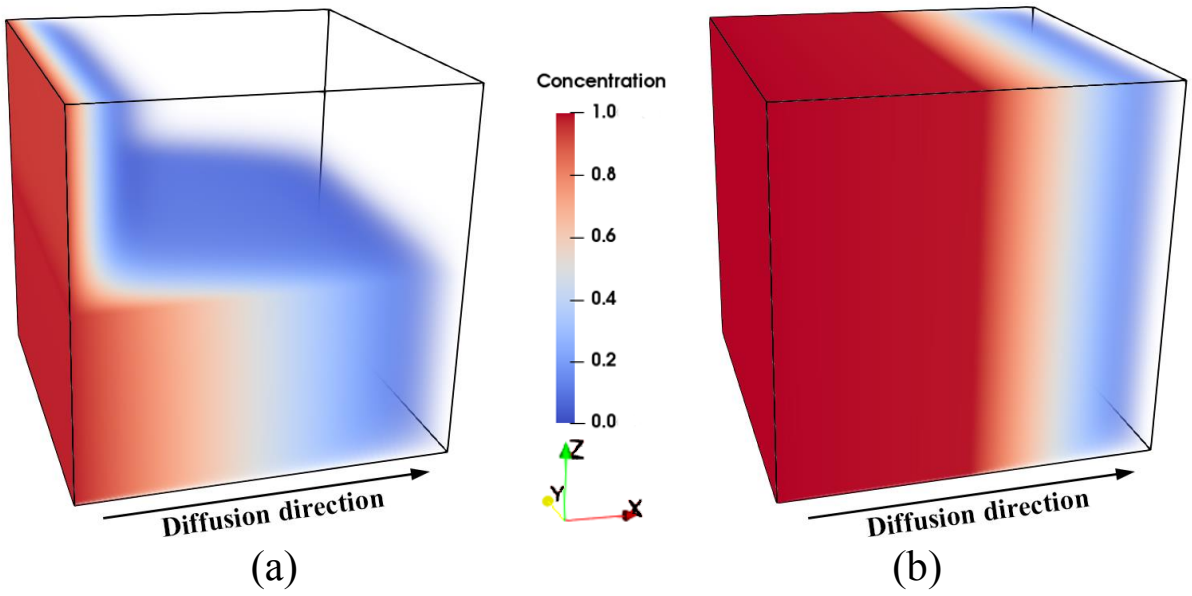

Fig. 4. Distribution of ionic concentration under steady-state condition (D_2/D_1=0.01): (a) parallel mode, and (b) series mode.

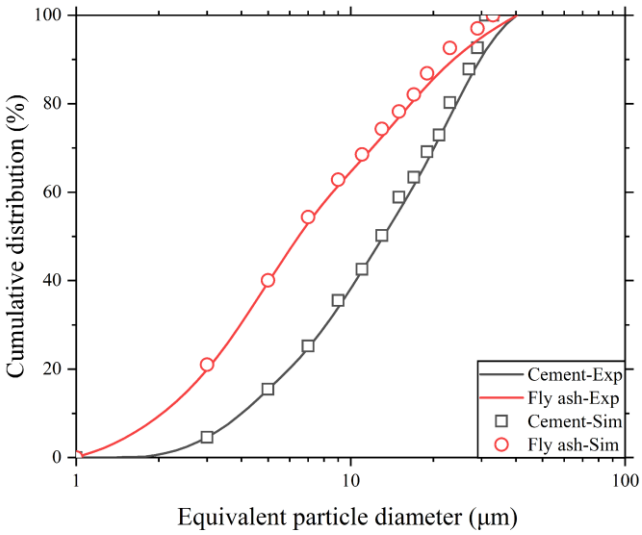

Fig. 5. Experimental and simulated particle size distribution of Portland cement and fly ash.

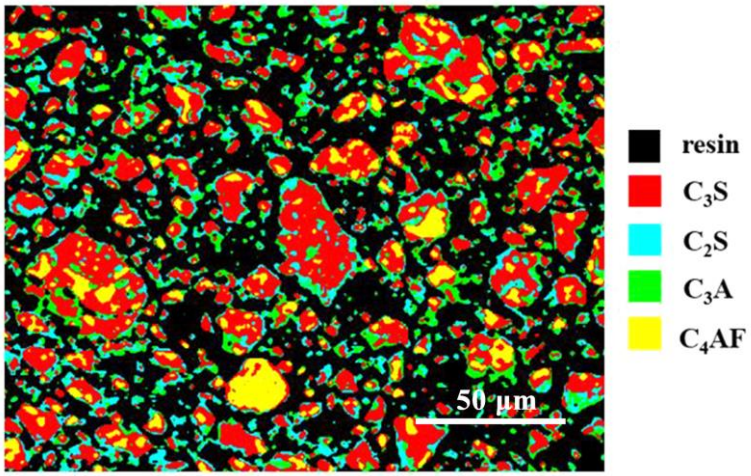

Fig. 6. A segmented SEM image of real cement powder with 512×400 pixels.

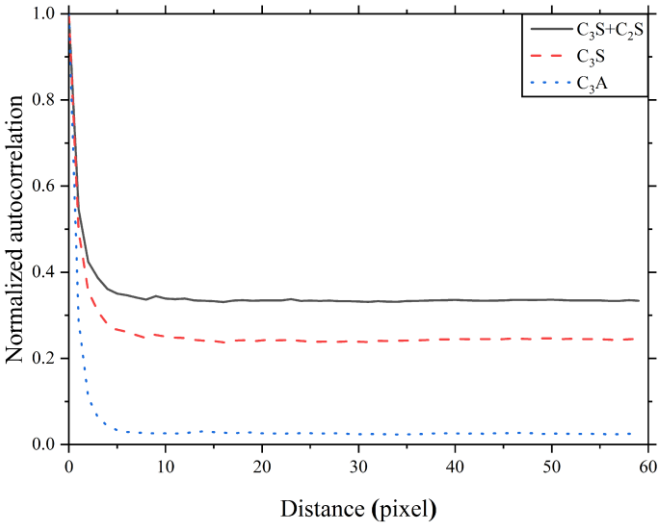

Fig. 7. Normalized autocorrelation functions of silicate (C_3S+ C_2S), C_3S and C_3A.

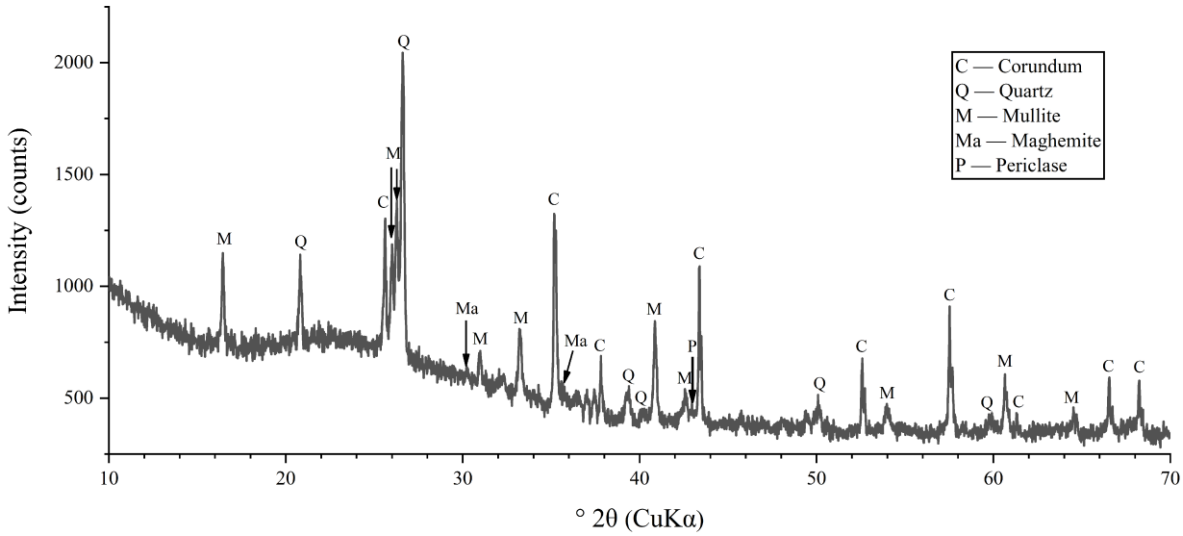

Fig. 8. XRD pattern of fly ash mixture with 10% pure corundum powder.

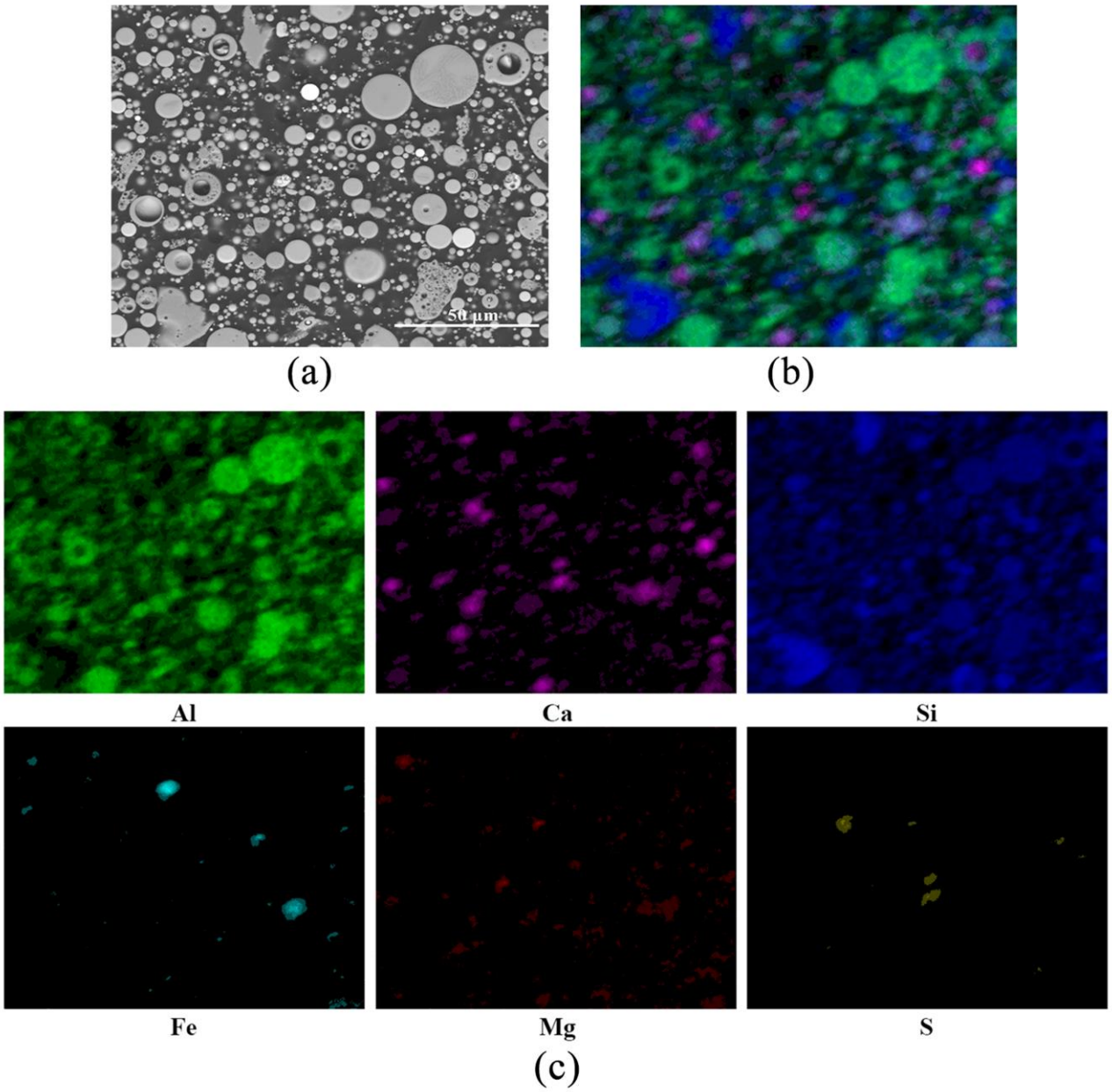

Fig. 9. (a) Backscatter electron image of fly ash; (b) ternary Al-Si-Ca distribution on fly ash; and (c) element mapping images of fly ash.

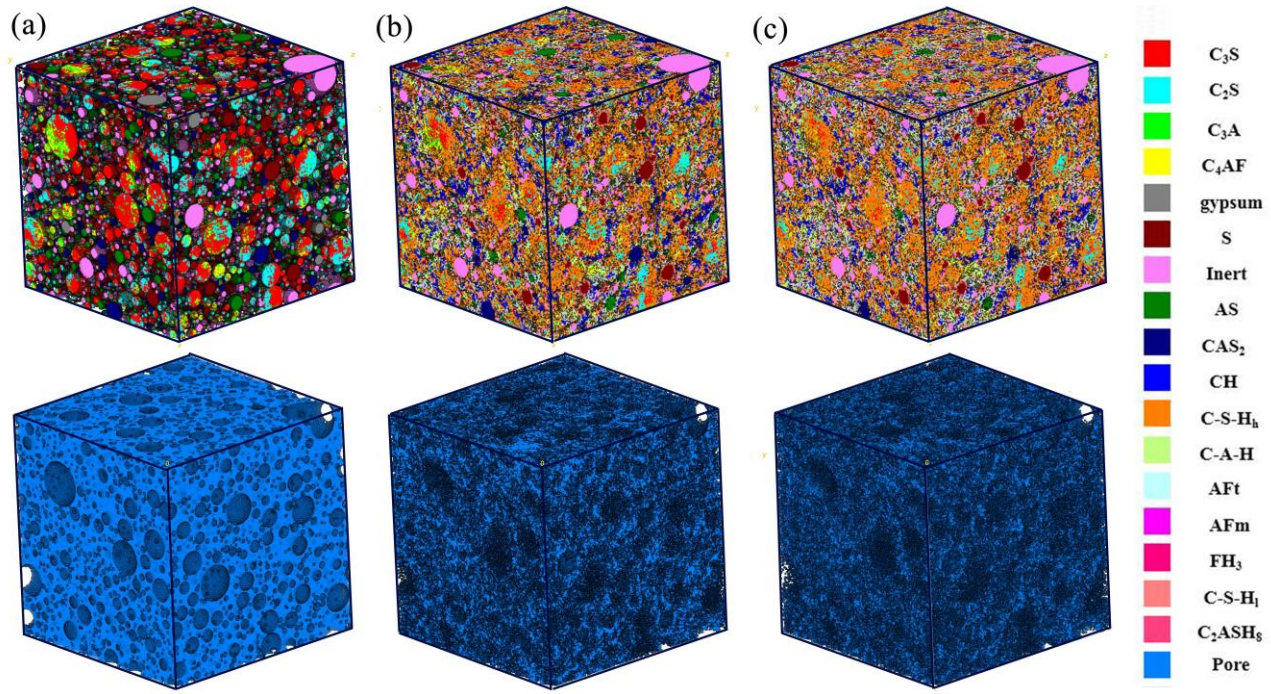

Fig. 10. Microstructure of fly ash blended cement pastes with w/b = 0.5 and 30% fly ash replacement ratio at (a) 0 d, (b) 28 d, and (c) 120 d (top row – solid, bottom row – capillary pore).

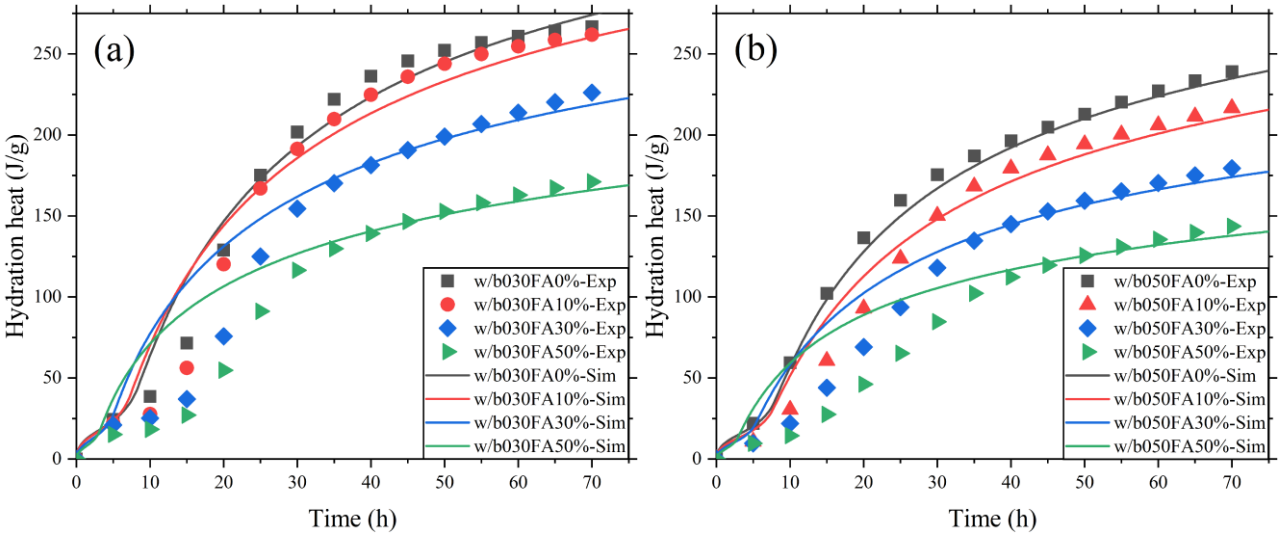

Fig. 11. Experimental and simulated hydration heat of fly ash blended cement pastes with w/b ratios of (a) 0.3, and (b) 0.5.

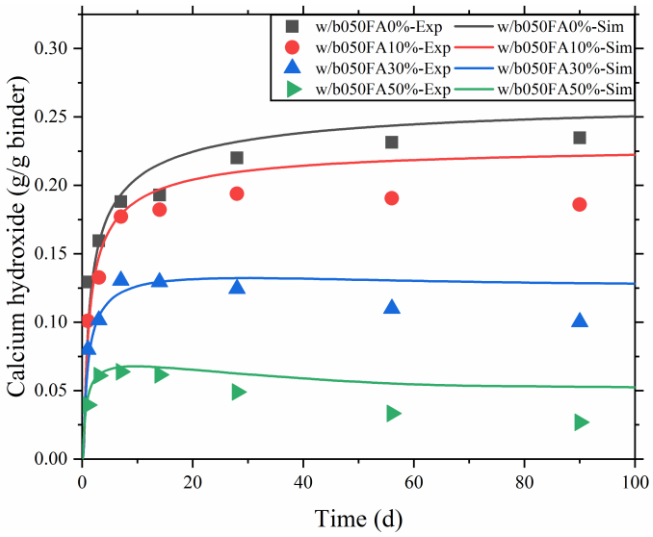

Fig. 12. Experimental and simulated calcium hydroxide content of fly ash blended cement pastes against curing age.

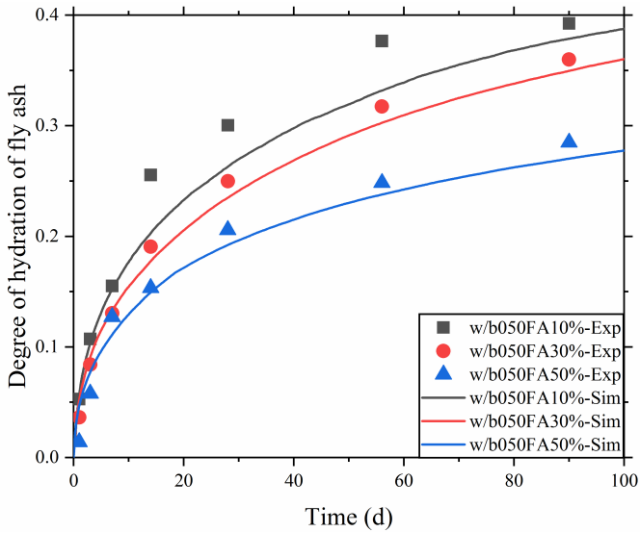

Fig. 13. Experimental and simulated degree of hydration of fly ash in pastes against curing age.

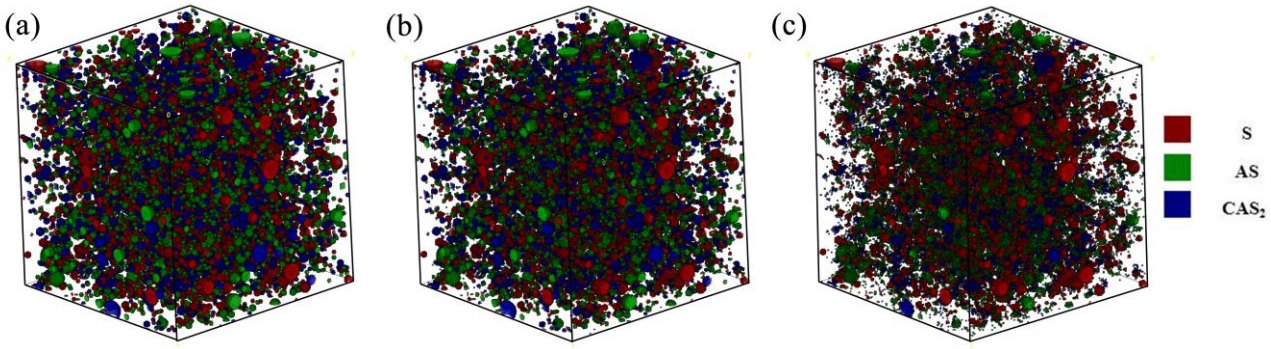

Fig. 14. Evolution of amorphous phases in fly ash in paste with w/b = 0.5 and 30% fly ash replacement ratio at (a) 0 d, (b) 7 d, and (c) 90 d.

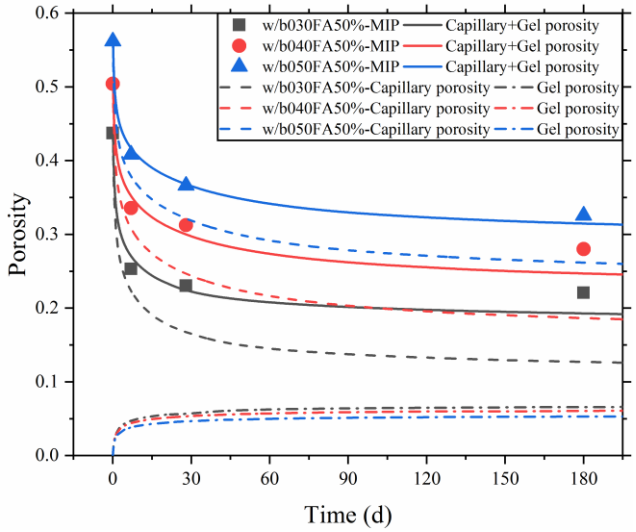

Fig. 15. Experimental and simulated porosity of fly ash blended cement pastes against curing age.

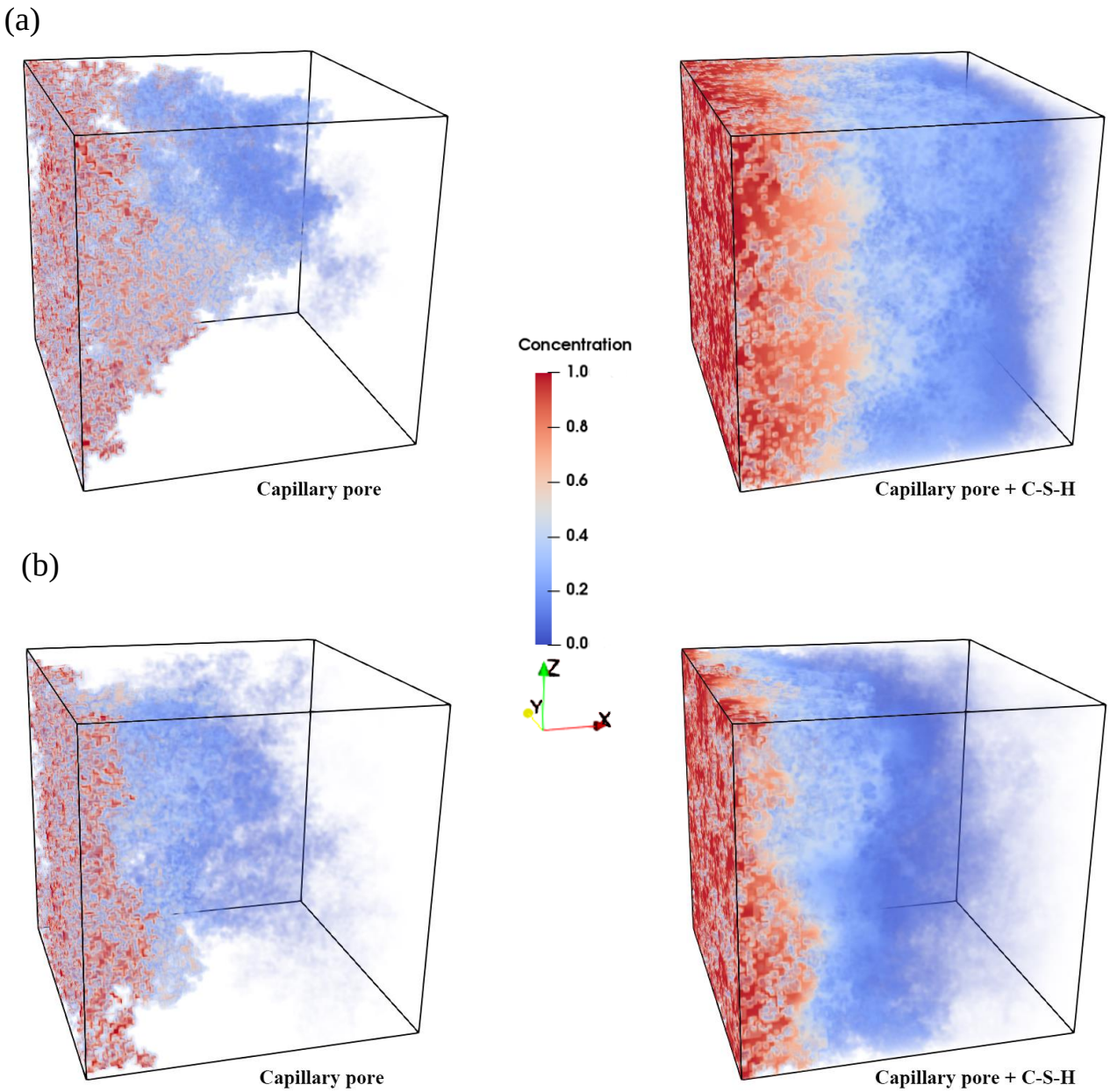

Fig. 16. Ionic concentration distribution at steady state in capillary pore network and microstructure including capillary pore and C-S-H of cement pastes at 120 d with fly ash replacement ratios of (a) 0%, and (b) 20%.

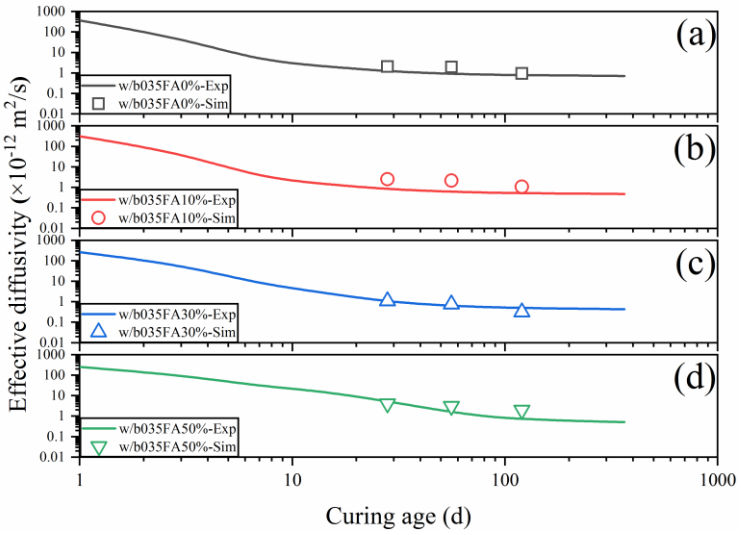

Fig. 17. Effective diffusivity of fly ash blended cement pastes with fly ash replacement ratios of (a) 0%, (b) 10%, (c) 30%, and (d) 50%.

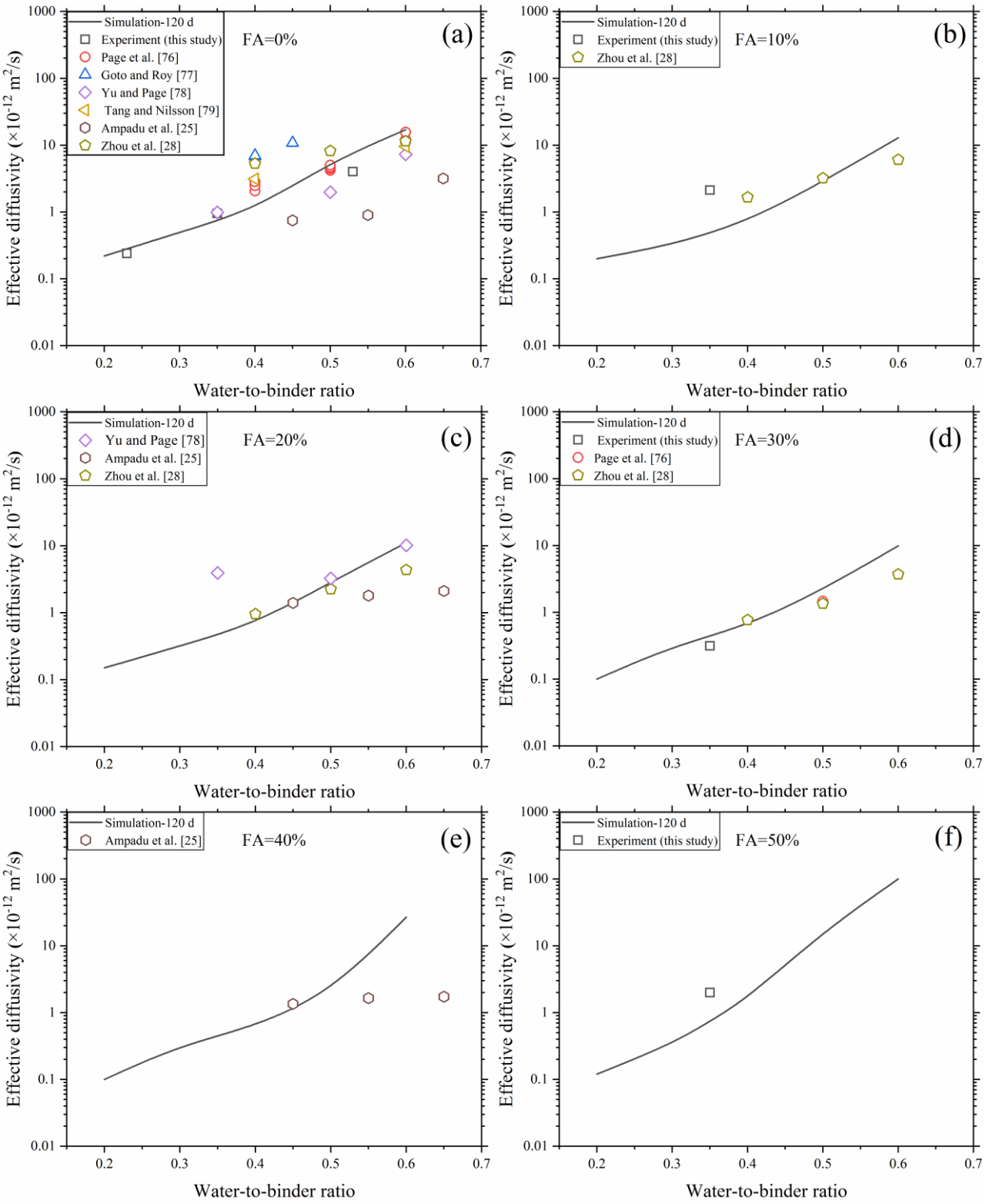

Fig. 18. Effect of w/b ratios on effective diffusivity of fly ash blended cement pastes with various fly ash replacement ratios.

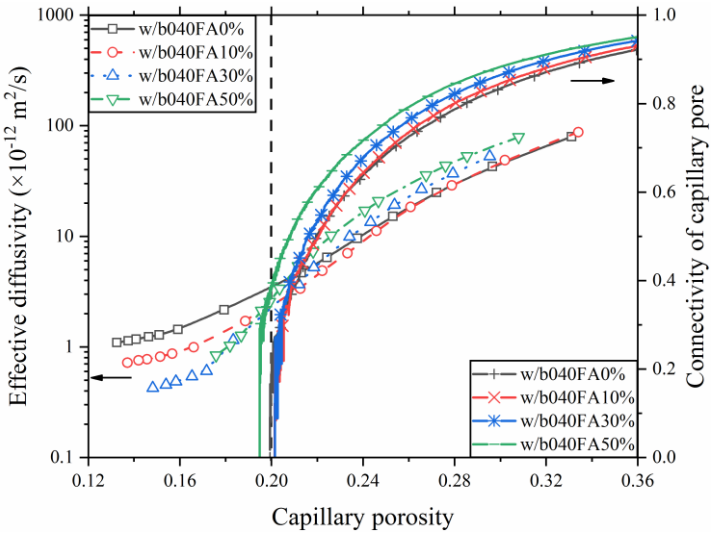

Fig. 19. Effective diffusivity and connectivity of capillary pore in fly ash blended cement pastes against capillary porosity.

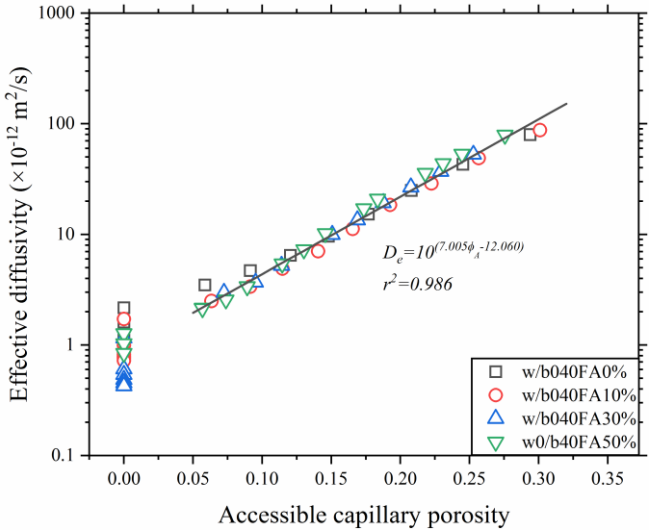

Fig. 20. Relationship between effective ionic diffusivity and accessible capillary porosity of fly ash blended cement pastes.

Table 1 Comparison of predicted results and theoretical solutions

D_2/D_1	Parallel mode			Series mode		
	Predicted value (m^2/s)	Theoretical value (m^2/s)	Relative deviation (%)	Predicted value (m^2/s)	Theoretical value (m^2/s)	Relative deviation (%)
0.5	0.75006	0.75	0.000	0.66728	0.66667	0.091
0.1	0.55004	0.55	0.007	0.18141	0.18182	0.225
0.01	0.50507	0.505	0.014	0.01987	0.01980	0.354
0.001	0.50052	0.5005	0.004	0.00201	0.00200	0.500
0.0001	0.50003	0.50005	0.006	0.00020	0.00020	0

Table 2 Chemical compositions and physical properties of Portland cement and fly ash

Chemical composition/physical properties	Cement	Fly ash
Calcium oxide (CaO, %)	64.47	4.09
Silicon dioxide (SiO_2, %)	21.37	47.86
Aluminum oxide (Al_2O_3, %)	4.87	32.50
Iron oxide (Fe_2O_3, %)	3.59	4.52
Magnesium oxide (MgO, %)	2.13	1.05
Sulfur trioxide (SO_3, %)	2.25	0.20
Sodium oxide (Na_2O, %)	0.11	0.55
Potassium oxide (K_2O, %)	0.35	1.62
Loss on ignition (LOI, %)	0.95	3.10
Blain fineness (m^2/kg)	369	454
Density (g/cm^3)	3.15	2.21

Table 3 Volume fractions of different phases in fly ash

Phase	Crystalline phase					Amorphous phase		
	Quartz (SiO_2)	Mullite ($Al_6Si_2O_{13}$)	Periclase (MgO)	Maghemite (Fe_2O_3)	Anhydrite ($CaSO_4$)	CAS_2	S	AS
Content (vol%)	23.1	11.5	0	2.4	0.4	19.3	22.4	20.9

Table 4 Summary of experimental studies on ionic diffusivity in hardened cement pastes

Ref.	Binder	Specimen	w/b ratio	Curing conditions	Test
This study	PC, PC+10%FA, PC+30%FA, PC+50%FA	Paste	0.23, 0.35, 0.53	20 ± 2 °C, relative humidity>95% for 120 d	Electro-migration (Steady-state)
Page et al. [76]	PC, PC+30% FA	Paste	0.4, 0.5,0.6	Saturated $Ca(OH)_2$ solution at 22 °C for 60 d with a three-week period of measurement	Diffusion cell
Goto and Roy [77]	PC	Paste	0.3, 0.35, 0.4, 0.45,	Saturated $Ca(OH)_2$ solution at 27 °C for three months	Diffusion cell
Yu and Page [78]	PC, PC+20%FA	Paste	0.35, 0.5, 0.6	Saturated $Ca(OH)_2$ solution at 22 °C for 3 months	Diffusion cell
Tang and Nilsson [79]	PC	Paste	0.4, 0.6	Saturated $Ca(OH)_2$ solution at 22 °C for 90 d	Diffusion cell
Ampadu et al. [25]	PC, PC+20%FA, PC+40%FA	Paste	0.35, 0.45, 0.55	Water at 20 °C for 91 d	Electro-migration (Steady-state)
Zhou et al. [28]	PC, PC+10%FA, PC+20%FA, PC+30%FA	Paste	0.4, 0.5, 0.6	20 ± 1 °C, relative humidity>95± 1% 120 d	Electro-accelerated test

Note: PC-Portland cement; FA-fly ash.